JPRS-JST-91-026
20 AUGUST 1991

Foreign Broadcast Information Service 50 ANNIVERSARY 1941 - 1991



# JPRS Report

# Science & Technology

## Japan

NEW DEVELOPMENTS IN ADVANCED MATERIALS

JPRS-JST-91-026
20 AUGUST 1991

# SCIENCE & TECHNOLOGY
# JAPAN

## NEW DEVELOPMENTS IN ADVANCED MATERIALS

916C0027 Tokyo KENKYU KOENKAI YOSHISHU in Japanese 19 Mar 91 pp 1-50

[Selections from FY90 Government Industrial Research Institute, Kyushu Seminar-Proceedings on Advanced Materials held 21 Feb 91 in Kagoshima and 19 Mar 91 in Kitakyushu; sponsored by the Kyushu Industrial Technology Center]

### CONTENTS

# Highly Functional Ceramics Through Structural Control of Grain Boundary Electronic Properties

916C0027A Tokyo KENKYU KOENKAI YOSHISHU in Japanese 19 Mar 91 pp 19-25

[Article by Makoto Kuwahara, Department of Engineering, Kyushu Institute of Technology: "Production of Highly Functional Ceramics Through Structural Control of Grain Boundary Electronic Properties and Its Practical Application"]

[Text] **1. Introduction**

Ceramics manifests its electronic properties as a compound phenomenon of electronic properties associated with the conditions within the grains and grain boundaries. This draws attention to ceramics for its possibility of generating unusual electronic properties that could not be expected from a single crystal. To apply the properties to the development of ceramic electronic materials, efforts to further enhance the new nonlinear electronic properties attributed to the grain boundary electronic properties are particularly important. In this section, I describe the varistor characteristic in ZnO-system ceramics, where the characteristic is manifested through the presence of the grain boundary and the crystal phase domain that could not be found in a single crystal, the positive temperature characteristic of resistance (PTCR) in barium titanate semiconductor ceramics, and the relaxer dielectric characteristic in compound-structure ferroelectric ceramics. The varistor properties of the ZnO-system ceramics have already been used in many practical applications. These properties and characteristics display a marked dependency on the structural conditions, which makes proper controlling of ceramic structure very important to realize an optimum grain boundary condition for generating the grain boundary electronic properties suitable for producing electronic application materials. In the following sections, I describe the structural dependency of the grain boundary electronic properties, the methods for structural control in ceramic production, and the practical use of highly functional ceramics.

**2. Ceramic Structure and the Energy Band**

Figure 1 shows the schematic representation of two typical ceramic structures with each having an insulation layer between adjoining n-type semiconductive

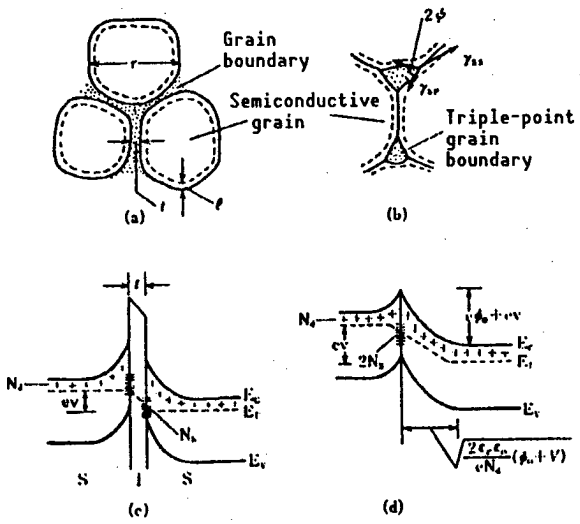


Figure 1. Schematic Representation of Material and Energy Band Models in Semiconductive Ceramics
(a) A case when grains are separated with a grain boundary insulation layer having a thickness of t, and
(b) A case in which a secondary phase was formed in the triple-point grain boundary with the value of t at zero.

grains and an energy band. Figure 1(c) shows a condition in which an insulation layer with a thickness of t exists between semiconductive grains having a grain diameter of r, with a voltage applied to the layer, and a condition in which an electron depletion layer with a width of 1 is formed on the grain surface. In the figure, it is assumed that an ionized region having a donor density of $N_d(cm^{-3})$ exists within the grain, and a surface acceptor region with a density of $N_s(cm^{-2})$ exists in the boundary between the insulation layer and the depletion layer, forming a superconductor-insulator-superconductor (SIS) structure. In the current flowing through the thin insulation layer, there are several types of current. Among them, Schottky-type current, Pool Frenkel-type current, and tunnel effect current are known to have a greater effect on the mechanism responsible for the extraordinary grain boundary electronic properties.

Figure 1(b) represents a state when t is zero. When no voltage is applied, the level of electric potential in the grain boundary barrier $e\phi_0$ is given by

$$e\phi_0 = e^2N_s^2/2\epsilon_r\epsilon_0N_d \qquad (1)$$

where e represents electron charge, $\epsilon_0$ represents vacuum dielectric constant, and $\epsilon_r$ represents relative dielectric constant (hereafter to be referred to simply as dielectric constant) in the grain boundary layer. Figure 1(b) also shows the presence of a secondary phase or pores in the triple-point grain boundary region. This condition is represented by a dihedral angle ($2\Psi$) dictated by the values of intergrain surface energy levels of $\gamma_{ss}$ and $\gamma_{sp}$ under a sinter condition.

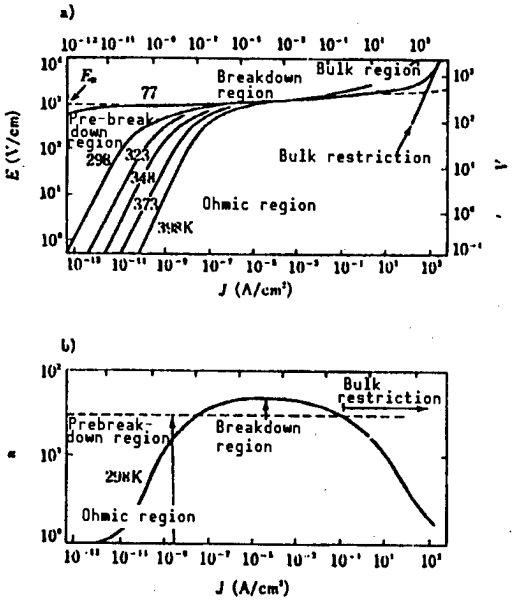


Figure 2. Example of Typical Varistor Characteristic in a ZnO-System Ceramics

When the triple-point grain boundary phase is made up of a pore, different grain boundary electronic properties could result depending on whether the pore pierces the material (open pore) or not (closed pore).

### 3. ZnO-System Ceramic Varistor

It has been found that introduction of impurities, mainly composed of $Bi_2O_3$, into compound ZnO semiconductive ceramics produces a remarkable nonlinear current-voltage characteristic (varistor characteristic) as shown in Figure 2. It has been found that the compound ceramics has a material structure similar to Figure 1(a) in which ZnO grains are separated with a $Bi_2O_3$-system insulation layer.

Usually, the current-voltage characteristic shown in Figure 2 is represented with an equation, $J = KE^{\alpha}$, where J denotes a current density, E an electric field strength, K a constant, and $\alpha$ a nonlinear index. The varistor characteristic is evaluated with the value of $\alpha$. Already, ceramics having such large $\alpha$ values ranging from 50~80 in the breakdown region has been developed and is being used in practical applications. It is known that $\alpha$ value fluctuates over a wide range depending on the microstructure in the grain boundaries and the chemistry involved. Particularly, the density of the surface acceptor level and the way in which it is present in the boundary region affects $\alpha$ level greatly. In addition, it is known that the introduction of MnO or CoO into ceramic material enhances the characteristics of highly functional ceramics significantly.

### 3.1 Varistor Structure in ZnO-System Ceramics

A number of energy band models that would help realize the varistor characteristic shown in Figure 2 have been announced. Among them, a Schottky/ grain boundary insulation layer/Schottky model is accepted commonly as a model that explains varistor structure well. The energy band condition for the model can be represented by one similar to Figure 1(c), in which the t value is so thin that it allows the current flowing through the insulation layer to take the form of a tunnel effect current.

### 3.2 Production of ZnO-System Ceramic Varistor and Its Practical Application

ZnO-system ceramic varistors are being manufactured using the conventional method. The varistor characteristic obtained varies greatly depending on the kinds of additives and their amounts introduced into varistor material and sinter conditions. Table 1 gives some typical varistor characteristics obtained using different kinds of additives and different sinter temperatures.

Table 1. Kinds of Additives and Varistor Characteristic

| Composition (mol%) | Sinter temperature (°C) | Varistor voltage ($V_{1mA}$/mm) | Nonohmic $\alpha$ index |
|---|---|---|---|
| ZnO 99.5<br>$Bi_2O_3$ 0.5 | 1,150 | 10 | 5 |
| ZnO 99.5<br>$Bi_2O_3$ 0.5<br>$Co_2O_3$ 0.0 | 1,250 | 30 | 15 |
| ZnO 99.0<br>$Bi_2O_3$ 0.5<br>$MnO_2$ 0.5 | 1,350 | 40 | 20 |
| ZnO 97.0<br>$Bi_2O_3$ 0.5<br>$Sb_2O_3$ 1.0<br>$Co_2O_3$ 0.5<br>$MnO_2$ 0.5<br>$Cr_2O_3$ 0.5 | 1,350 | 160 | 55 |
| ZnO 96.5<br>$Bi_2O_3$ 0.5<br>$Sb_2O_3$ 1.0<br>$Co_2O_3$ 0.5<br>$MnO_2$ 0.5<br>$Cr_2O_3$ 0.5<br>$SiO_2$ 0.5 | 1,350 | 220 | 55 |

From the table, it is clear that introducing Mn or Co is effective in enhancing nonlinear $\alpha$ index substantially, making it possible to improve varistor characteristic greatly. It is believed that the improvement is realized by introducing these elements, contributing to the generation of a surface acceptor level, as indicated in Figure 1(c) and (d), and, in turn, working effectively in lowering current level in the ohmic region.

So far, many kinds of varistor materials have been developed and some of them have been put to practical use. Among them, ZnO-system materials are used most popularly in varistor production because of their superior characteristics and wider application range.

Figure 3 gives the systematic application fields of ZnO-system varistors. The products cover very wide ranges in usable voltages and frequencies ($10^{-3}$~$10^{5}$ V, $10^{-3}$~$10^{5}$ MHz). When compared with other p-n junction varistors or SiC varistors, it can be seen that ZnO-system counterparts are far superior because they are used at a wider operation range.

## 4. PTCR Effect in Barium Titanate Semiconductive Ceramics

Barium titanate ($BaTiO_3$) is a ferroelectric substance having a Curie point at around 120°C, and pure barium titanate has a resistivity higher than $10^{10}\Omega$cm at room temperature. By adding elements such as La or Sb of 0.1~0.3 at%, barium titanate becomes semiconductive displaying a large PTCR at a temperature higher than the Curie point.

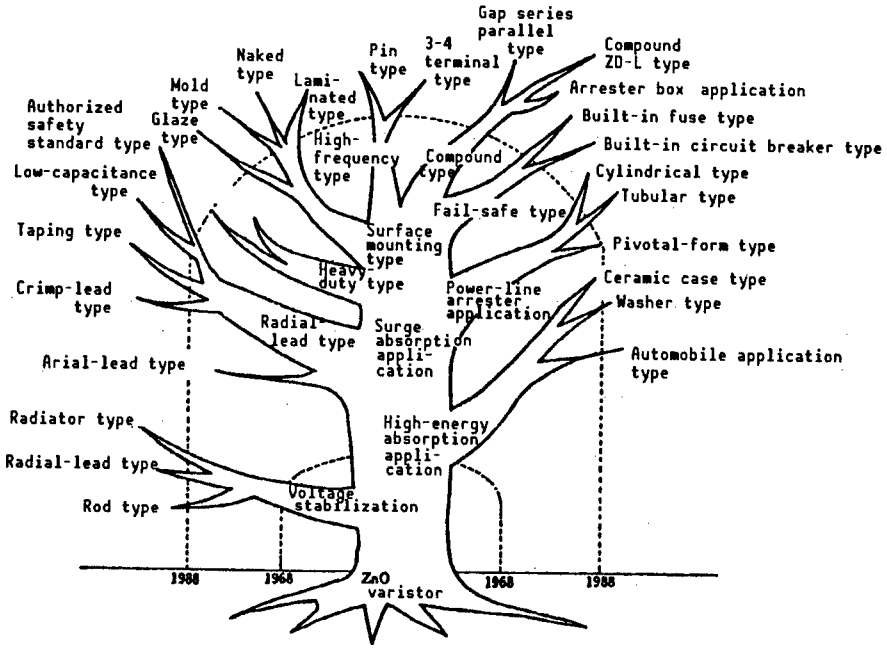


Figure 3. ZnO-System Varistor's Application Fields

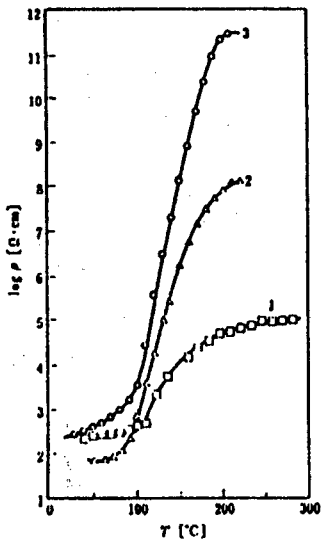


Figure 4. Three Typical Types of PTCR Characteristics Observed in Barium Titanate Semiconductive Ceramics
Curve 1: Large grain-diameter, high-density material;
Curve 2: Mn-containing material currently available on the market;
Curve 3: Porous small-diameter grain material.

The PTCR effect is one of the typical grain boundary electronic properties in ceramics, and the ceramics displaying such an effect is believed to have a microstructure and an energy band condition similar to the one shown in Figure 1(b) and (d), respectively.

Figure 4 shows the three typical types of PTCR characteristics observed in $BaTiO_3$-system semiconductive ceramics. In the figure, curve 1 represents the PTCR characteristic of a material produced using the conventional sintering method and having high-density, large-diameter grains; curve 2 is for a material currently available on the market and contains a tiny amount of MnO as an additive to improve PTCR effect; and curve 3 is the PTCR characteristic for a material developed by this author's research group that has a porous small-diameter grain structure. The figure shows that the manifestation of PTCR effect in ceramics depends greatly on the material structure. Consequently, it is very important to establish a grain boundary microstructure controlling technique and to promote research on the chemistry associated with the surface acceptor level to unravel the PTCR effect mechanism and to further enhance the effect.

### 4.1 Mechanism of PTCR Effects

The PTCR effect in $BaTiO_3$-system semiconductive ceramics can be explained using the grain boundary barrier layer model proposed by Heywang. According to the model, a decrease in the dielectric constant $\epsilon_r$ in the electron depletion layer on the $BaTiO_3$ semiconductive grains in accordance with the Curie-Weiss law above the Curie point temperature causes an increase in the potential level (represented by $e\phi_0$ in Equation (1) in the grain boundary barrier layer.

This, in turn, causes a steep rise in the resistivity $\rho$ under a low electric field strength in ceramics above the Curie point temperature. In the model, the value $\rho$ is given as

$$\rho = \rho_0 \exp (e\phi_0/kT) = \rho_0 \exp (A/\epsilon_r T) \quad (2)$$

where $\rho_0$ denotes the resistivity within material grains and A represents a constant. In the model, the presence of a surface acceptor level is required to form the grain boundary barrier layer.

### 4.2 Production of Barium Titanate Semiconductive Ceramics and its Practical Application

Barium titanate semiconductive ceramics is being produced using a conventional ceramic manufacturing method. By changing the ingredient materials and the production process, ceramics having different material structures and different PTCR characteristics can be manufactured. The two types of ceramics, whose characteristics are given in Figure 4(1) and (3), have different material structures. Their microstructure scanning electron microscope (SEM) images are shown in Figure 5. Figure 5(a) shows the surface condition and the cross section view of a ceramics whose characteristic is represented by the curve 1 in Figure 4. It has been found that another type of ceramics having a less impressive PTCR characteristic has a more complex and less clear grain profile, though it displays a clear grain profile on the ceramic surface. On the other hand, as shown in Figure 5(b), porous ceramics displays a clear grain profile on the surface. The grain structure in the porous ceramics resembles one shown in Figure 1(b), in which the triple-point grain boundary layer contains open pores. In producing ceramics, it is important to adopt a method that allows control of the microstructure.

PTCR ceramics is popularly used in producing temperature sensors, stabilized-temperature heaters, and color TV demagnetizing devices by taking advantage of the unique current-voltage, temperature-resistance, and time-current characteristics. Table 2 gives the principal application fields of PTCR materials.

## 5. Relaxer-Type Dielectric Characteristic in Compound Ferroelectric Materials

Ferroelectric materials composed of a single material, like $BaTiO_3$ and $KNbO_3$ ceramics, display a sharp increase in dielectric constant at their Curie points. However, compound ferroelectric materials like $Pb(Mg_{1/3}Nb_{2/3})O_3$ (PMN) are known to have less sharp and lower dielectric constant increases (Figure 6) that have a great frequency dependency (relaxation) near their Curie points. These compound ferroelectric materials are called relaxer, which exhibits high dielectric constant values affected little by temperature variation.

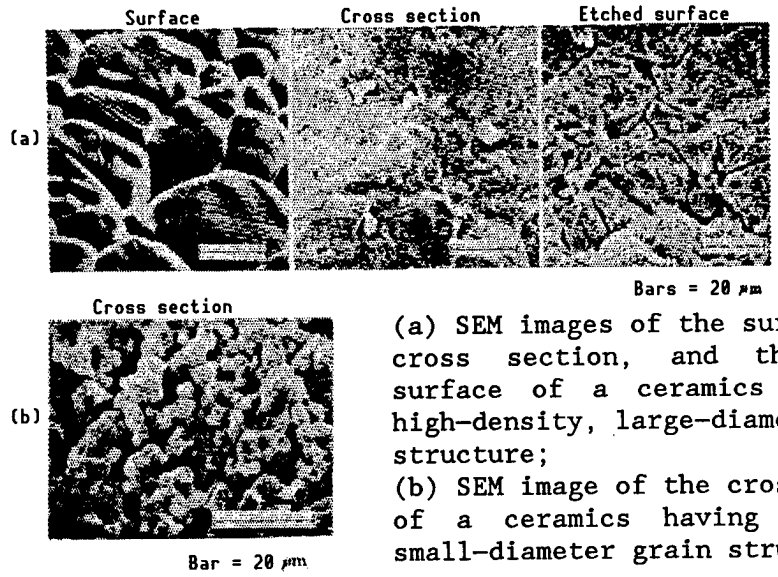


(a) SEM images of the surface, the cross section, and the etched surface of a ceramics having a high-density, large-diameter grain structure;
(b) SEM image of the cross section of a ceramics having a porous small-diameter grain structure.

Figure 5. Typical Microstructure SEM Images in Ceramic Samples That Have PTCR Characteristics Represented by the Curves 1 and 3 in Figure 4.

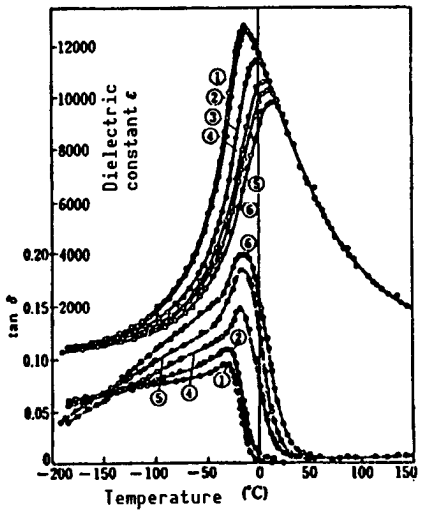


Figure 6. Frequency Dependency of Temperature-Dielectric Constant in $Pb(Mg_{1/3}Nb_{2/3})O_3$ Ceramics

Table 2. Principal Application Fields of PTCR Thermistors

| | | |
|---|---|---|
| Use of temperature-resistance characteristic | Temperature compensation element | Various electronic equipment circuit application |
| | Temperature sensor | Temperature controlling in electric foot warmer |
| Use of current voltage characteristic | Stabilized-temperature heater | Electronic rice cooker, removal of water within the cooker, butter heater in refrigerator, electronic mosquito killer, electric incense burner, electronic foot warmer, electronic boots, copier, facsimile fixer heater, prevention of dew formation in VCR, hair iron, freeze-prevention heater, oil vaporization heater, auto choke heater, air valve heater |
| | Warm wind generating heater | Household room heater; car compartment heater; dishes, clothes, and bedding dryer; hair dryer; foot warmer |
| Use of time-current characteristic | Demagnetizing device | Color TV set, color display tube |
| | Element for motor starting | Refrigerator, air compressor |
| | Excessive current flow prevention | Motor, relay coil, electronic circuit, fluorescent lamp |
| | Timer | Buzzer, lamp |

In recent years, relaxer-type ferroelectric materials have been drawing increasing attention as high dielectric constant materials, and some of them are already being used in practical applications. PMN has a large electrostriction coefficient and draws attention as a good electrostriction material. The difference between a crystalline phase transformation (DPT), responsible for such a superior dielectric characteristic, and normal phase transformation (NPT), responsible for a sharp surge of dielectric constant, is believed to result from differences in microstructures in the spontaneous polarization domain, i.e., due to the differences in the type and size of the microstructures.

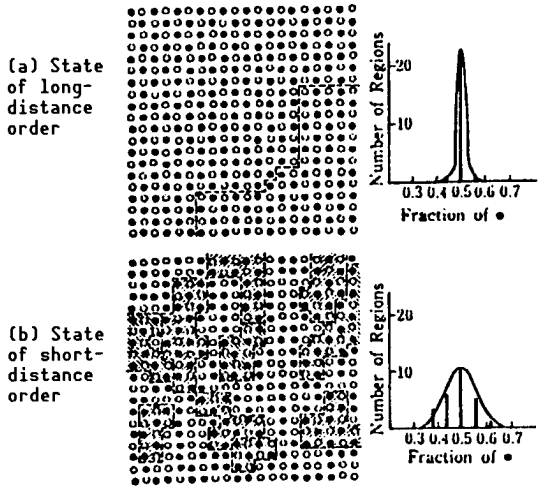


Figure 7. Regular Configuration of B-Site Ions in $A(B^{I}_{1/2}B^{II}_{1/2})O_3$ Ceramics and a Compositional Change

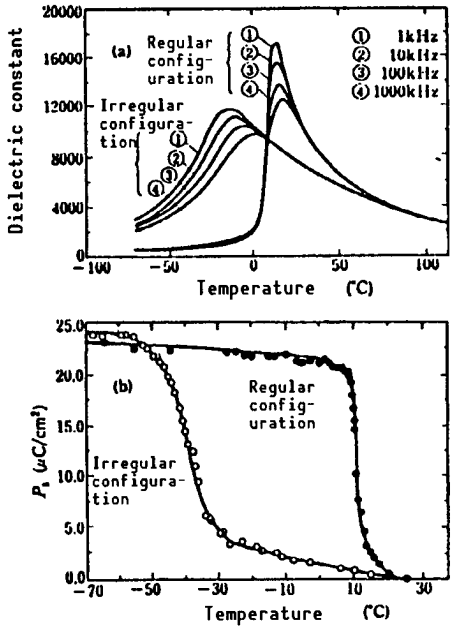


Figure 8. Temperature Dependency of (a) Dielectric Constant and (b) Spontaneous Polarization in $Pb(Sc_{1/2}Ta_{1/2})O_3$ Having a Regular Single Crystal Configuration and an Irregular Single Crystal Configuration, Respectively

### 5.1 Manifestation Mechanism in Relaxer-Type Dielectric Characteristic

The sharp surge in dielectric constant as a result of an NPT occurs as a cooperative phenomenon in the macroscale motion of pipole moment. At first, the broad peaking in the increase of dielectric constant as a result of a DPT was explained by Smolenskii as being caused by the statistical distribution of Curie point accompanying a localized composition change occurring within a crystallized material (Figure 7). On the other hand, Cross, et al., announced that in the B-site atomic configuration, there exists a nanolevel order-disorder domain. They explain that the increase is caused by the statistical thermodynamic motion in the polarized domain.

Cross, et al., announced that through experiments using $Pb(Sc_{1/2}Ta/_{1/2})O_3$ (PST) (Figure 8) they confirmed that the state of order-disorder configuration in the B-site atoms decides whether a ceramics' dielectric characteristic takes an NPT or a DPT form. However, there are still problems that have yet to be resolved to clarify the configuration. To unravel the mechanism in the manifestation of DPT dielectric characteristic and to improve the characteristic further, more effort must be made to clarify the domain microstructure in ceramics.

### 5.2 Production of Relaxer-Type Ferroelectric Material and Its Practical Application

The most important thing in producing compound ferroelectric materials is to ensure the uniform distribution of the ingredient components in mixing them together. To realize a uniform distribution, various methods have been developed. One of them involves subjecting the starting materials to a long mixing process. To improve uniformity, the oxalate method and sol-gel methods are also used, in which mixing starts using liquid-phase materials.

Relaxer-type ferroelectric materials, having a high dielectric constant and the constant's small temperature dependency, are suitable for application where these merits can be taken advantage of. These materials can be produced at comparatively low sinter temperature, and this allows them to be used popularly in manufacturing multilayer capacitors. Considering the low sinter temperature involved, demand for these materials is expected to continue to increase in the future.

## 6. Epilogue

So far in this article, I have discussed the varistor characteristic in ZnO-system ceramics, the PTCR characteristic in barium titanate semiconductive ceramics, and the relaxer-type dielectric characteristic in compound ferroelectric ceramics and the dependency of these characteristics on ceramic microstructure. I have also introduced the production methods designed to promote these characteristics and the practical uses of these materials. In developing functional ceramics, it is very important to establish a production process capable of controlling ceramic microstructure to promote manifestation of new material properties and the functionality of ceramics, in addition to stepped-up efforts to clarify the relationship between ceramics' microstructure and electronic properties.

**Boron Nitride Ceramics Using Atmospheric Sintering**

916C0027B Tokyo KENKYU KOENKAI YOSHISHU in Japanese 19 Mar 91 pp 27-32

[Article by Tsuyoshi Hagio, Government Industrial Research Institute, Kyushu:
"Production of Boron Nitride Ceramics Using Atmospheric Sintering Method"]

[Text] **1. Introduction**

In recent years, research and development in the field of ceramics has centered on nonoxide ceramics to develop structural materials and electronics application materials. Engineering ceramics, silicon carbide ceramics, silicon nitride ceramics, and zirconia ceramics are drawing particular attention. In addition, there is high interest in aluminum nitride and boron nitride as nitride ceramics. Hexagonal boron nitride (h-BN) has a crystal structure similar to graphite and in many respects has properties similar to graphite. Both are good heat conductors, have a good lubricity and a high chemical resistivity, and are stable producing comparatively low vapor pressure up to 3,000°C when put into a reducing atmosphere. The fact that h-BN has a layer crystal structure similar to that of graphite gives it the name "white graphite." Hexagonal boron nitride began to be used in industrial applications about 15 years ago. At first, it was used in applications where heat and corrosion withstanding capabilities were required. However, in recent years, it has drawn increased attention for its superior electrical insulation and heat radiation capabilities, and demand for the material has been increasing sharply in the electronic field. Hexagonal boron nitride is a material that cannot be sintered easily, and because of this, the production of BN compacts has mainly used the hot press method. At this author's institute, effort has been made to develop a simpler BN compact production method in which sintering can be made under atmospheric pressure, and as a result, an atmospheric sintering method involving the use of ground BN powder has been developed. Boron nitride has a cubic variation in addition to hexagonal boron nitride. However, the following discussion will be restricted to the crystal structure of h-BN, the material's production method, and chemical properties. In addition, it will outline the atmospheric sintering method.

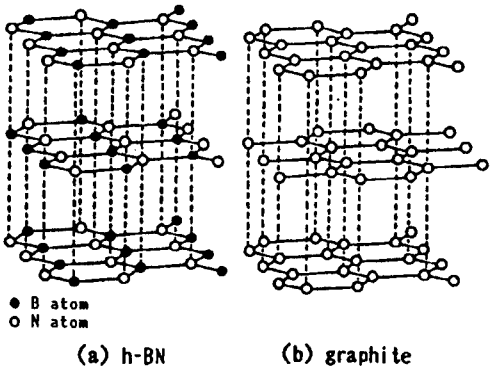


Figure 1. Crystal Structures of h-BN and Graphite

## 2. Chemical Properties of h-BN

Boron nitride is a compound composed of one boron atom and one nitrogen atom, and in the periodic table B and N are on either side of C. The crystal structural similarity makes boron nitride comparable to carbon, and so far, four different boron nitride crystal structures—hexagonal boron nitride (h-BN), rhombohedral boron nitride (r-BN), cubic boron nitride (c-BN), and wurtzite boron nitride (w-BN)—have been found.

Hexagonal boron nitride has a crystal structure similar to that of graphite, and it is composed of layers of hexagonal BN planes. Figure 1 shows the typical crystal structures of h-BN and graphite. The difference between the crystal structures of h-BN and graphite is the way in which the adjoining layers are aligned. In h-BN, the planes are aligned in such a way that N atoms on the adjoining planes are positioned immediately above and below a B atom on a given plane, whereas in graphite, the hexagonal planes above and below a given plane are shifted to one direction. The lattice constants in h-BN are $a = 2.5038$ A and $c = 6.66$ A, and the bonding distances between B and N are 1.45 A within a layer and a 3.33 A between layers. Though h-BN has properties closely resembling those of graphite due to the similarity of crystal structures, h-BN and graphite have completely different material colors and electrical characteristics. Table 1 gives the basic properties of h-BN, and the following section describes the typical features of the material.

**(Thermal Property)** Hexagonal boron nitride is a thermally stable substance and under a pressurized nitrogen atmosphere has a melting point higher than 3,000°C and a boiling point higher than 5,000°C. This allows h-BN to be used safely up to a temperature of 2,000°C in a vacuum atmosphere and to 2,200°C in an inert gas atmosphere. In an oxidizing atmosphere, oxidation begins at around 900°C. Hexagonal boron nitride has a thermal conductivity as high as that of steel, and the value is close to that of aluminum nitride, beryllia, and silicon carbide, a group of materials having particularly high thermal conductivities. The layer structure makes the thermal expansion coefficient show an anisotropy. However, h-BN compacts have comparatively small thermal expansion rates. The high thermal conductivity and the small thermal expansion coefficient make an h-BN compact display a superior antiheat shock capability,

Table 1. Basic Properties of Boron Nitride

| Item | Level |
|---|---|
| Theoretical density | 2.270 $g/cm^3$ |
| Melting point | >3,000°C ($N_2$ under pressurized nitrogen) |
| Boiling point | 5,060°C |
| Specific heat | 1.61 + 4.00 x $10^{-3}$T cal/mole.°C |
| Thermal expansion coefficient | 41 x $10^{-6}$ /°C (c axis direction)<br>-2.9 x $10^{-6}$ /°C (a axis direction) |
| Thermal conductivity | 2.9 W/m·K (c axis direction)<br>62 W/m·K (a axis direction) |
| Volume resistivity | $10^5$ Ωcm |
| Hardness | 2 Mohs |

and even when it is dipped into molten steel with a temperature of 1,500°C, no cracks appear on the compact.

**(Chemical Property)** Hexagonal boron nitride is a chemically inert substance and exhibits a high stability when it is exposed to a strong acid or organic solvent. The boron nitride does not react easily with iron, copper, brass, nickel, zinc, or gallium arsenide when it is exposed to these metals in molten form, and it also displays a good anticorrosion ability against glass or slag.

**(Electrical Property)** Hexagonal boron nitride has a large insulation resistance. At room temperature, it has a volume resistivity higher than $10^{14}\Omega\cdot cm$, and at a temperature of 1,200°C it still has a volume resistivity of $10^{7}\Omega\cdot cm$. As opposed to oxide ceramics, which loses its insulation capability at high temperatures, h-BN can be used as an electrical insulation material over a wide temperature range.

**(Lubrication Capability)** Hexagonal boron nitride has a friction coefficient and a solid lubricity as low as that of graphite of molybdenum disulfide. The good lubricity results from the fact that in h-BN the bonding strength between adjoining layers of the crystal is smaller than that between atoms within a layer, making the bonding between the layers easily broken when an external force is applied to the layer surface parallel to it. Graphite and molybdenum disulfide disintegrate at a relatively low temperature and lose lubricity when they are oxidized. Conversely, h-BN maintains a stable low friction coefficient even when it is put within a 900°C atmosphere, and it displays a superior capability as a solid lubricating material at high temperature.

## 3. h-BN Ceramics Production Methods

As with the case in producing various carbon-based materials, there are a number of forms in which h-BN ceramics is available industrially today. It is available in powder form, compact form, and thermal decomposition BN form. Attempts are being made to produce carbon black like BN, BN fiber, and compound BN/BN material. However, they are little used industrially.

**(Powder)** Ever since W.R. Balmain succeeded in synthesizing h-BN powder in 1842, many methods have been developed to produce h-BN in powder form. The method currently being used industrially calls for heating nitrogen-containing compounds like ammonia or urea together with boric acid anhydride or borate to synthesize BN. When heated, both boric acid anhydride and borate turn into a highly viscous fluid, and this reduces these chemicals' surface area for reaction with nitride gas. To prevent this, a number of measures have been devised, including introducing calcium phosphate as a carrier and having boric acid anhydride or borate react with urea at a low temperature to turn the mixture into a spongy form that is then vaporized at high temperature. Generally, the BN powder thus produced has a purity ranging from 80~90 percent depending on the production techniques and temperature involved. As minor components, the powder also contains isolated boric oxide, and within BN crystal B-N-O-system intermediate products are contained. The purity of BN powder containing these impurities and having a low degree of crystallization can be improved further by subjecting the powder to a heat treatment at a temperature ranging from 1,700~2,100°C within a nonoxidizing atmosphere of nitrogen or argon. The heat treatment vaporizes the impurities, including boric oxide, and this improves the crystallization in BN powder. By adding either boric oxide or carbon to the BN powder during the heat treatment, it is possible to control the purity, the grain diameter, and the crystallization in the synthesized h-BN powder. The good lubricity and chemical stability of BN powder at high temperature makes it popular in various industrial fields as a lubricant and as an agent to help remove a molded product from a molding machine. BN powder is also used in producing compound BN silicon rubber sheets, which are used as a spacer in mounting transistors and diodes on the substrates by taking advantage of the powder's high insulation resistance and high thermal conductivity to radiate heat generated by these semiconductor devices.

**(Compact)** Usually a BN compact is produced using the hot press method. The method involves boric oxide, silicon nitride, and aluminum phosphate as binding agents, and heating in a high-frequency induction furnace equipped with high-density graphite dies. In the hot press method, a BN compact is produced by heating the molded compact at around 2,000°C under a pressure of around 400 $kg/cm^2$. In producing a BN compact the adjustment of the starting materials is also important. By optimizing the hot press condition, a BN compact having a density higher than 2.0 $g/cm^3$ has been obtained without the use of a powder binder. The superior anticorrosion capability of a BN compact in molten metal handling allows it to be used in various kinds of crucibles for melting metal and in protective pipes for housing high-temperature application thermocouples.

The low wettability when in contact with molten glass allows BN compacts to be used in glass molding. BN compacts are also used in manufacturing transportation machinery parts, and their high insulation resistance and high thermal conductivity allow them to be used in producing heat-radiating substrates for mounting transistors and IC chips.

**(Thermal Decomposition BN)** Just like a graphite (PG) produced through a thermal decomposition of the starting materials, a BN (PBN) is being produced using a chemical vapor deposition (CVD) method involving a thermal decomposition process. The BN thus produced is being used to make the crucibles for growing GaAs single crystals and other kinds of compound semiconductive single crystals and to produce molecular beam epitaxy (MBE) cells, and application fields are expanding. Industrially, PBN is being produced by thermally decomposing boron halide and ammonia as the starting materials at a temperature higher than 1,000°C. Depending on the CVD condition used, synthesized PBN has different crystal structures and mechanical properties. For example, when synthesizing temperature is increased, the crystal structure within the synthesized PBN shifts from an amorphous structure to an irregular layer structure to a hexagonal structure. When reaction pressure is low, PBN is synthesized in a film form, and when pressure is increased substantially the synthesized product assumes a powdery form.

## 4. Sintering of BN Under Atmospheric Pressure

Hexagonal boron nitride is very difficult to sinter. Even when the hot press method is used, the BN compact density does not exceed 1.22 $g/cm^3$, only 54 percent of the theoretically attainable density. This is why only the hot press method has been used in producing h-BN compact. This author's research group had made efforts to develop a method that allows producing an h-BN compact under atmospheric pressure, and as a result, we found that giving a mechanochemical treatment to starting BN powder is useful to overcome the problem. The atmospheric sintering method developed by this author's group uses refined impurity-free BN powder.

### 4.1 Atmospheric Sintering Method

The atmospheric sintering method involves three principal processes—adjusting starting BN material powder, molding the powder into a desired shape, and sintering. Figure 2 shows the production procedure flow chart. When BN material is crushed into powder using a machine, an ammonia smell is produced and this leads to the synthesis of chemicals like ammonium of boric acid hydrate (Figure 3). The volume of these synthesized byproducts increases in proportion to the material processing time. When the BN powder containing them is molded and sintered, a bulge and cracks develop in the sintered compact. This required the material powder to be treated with methanol and other chemicals to remove the unwanted synthesized byproducts. The treatment produces a pure BN powder containing no crystallized compounds other than BN. Table 2 gives a comparison of properties between typical pulverized BN powder and untreated starting BN powder. The values for the pulverized BN powder were obtained after subjecting a crystallized and high-purity BN powder to a 48-hour treatment process.

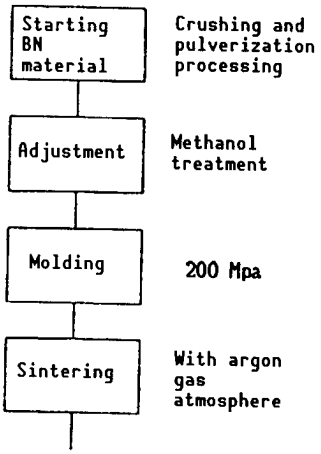


Figure 2. Process Flow Chart in Atmospheric Sintering Method

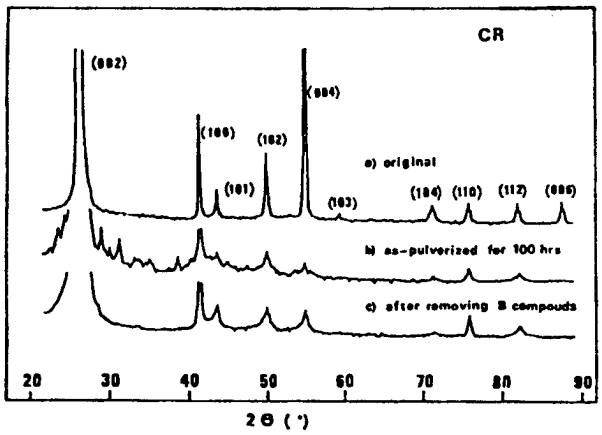


Figure 3. Results of X-Ray Diffraction Analysis
(a) Starting h-BN powder
(b) After pulverization
(c) After methanol treatment

Table 2. Properties of Pulverized Boron Nitride Powder

| Starting material | | Pulverized BN (48 h) | |
|---|---|---|---|
| Purity | (%) | 99.4 | 93.9 |
| Impurities (oxygen) | (%) | <0.1 | 5.0 |
| Grain size | (m) | 10 | 2 |
| Specific surface area | ($M^2$/g) | 5 | 100 |
| X-ray parameter | | | |
| $c_0$ | (A) | 6.66 | 6.66 |
| Lc(002) | (A) | <1000 | 500 |

Generally, pulverized BN powder has a round grain shape, and compared to the starting BN powder it has a more irregular crystal structure. The pulverized powder also contains more impure oxygen, and the grain has a larger specific surface area. These changes increase in proportion to the length of the treatment time, and a similar tendency can be observed apart from the differences in purity and crystal structure of starting BN powder. A sintered compact can be produced by molding the pulverized powder under a pressure of 200 MPa, enveloping the molded compact with a film of BN powder, and then sintering within an argon gas atmosphere. In the pulverization process, excessive time for starting powder processing is not recommended. Lengthened time of processing produced cracks on sintered BN compacts. In the experiment by this author's group, we used a crusher in the pulverization process. A vibration bowl mill or an (atoraita) can also be used as a crushing machine.

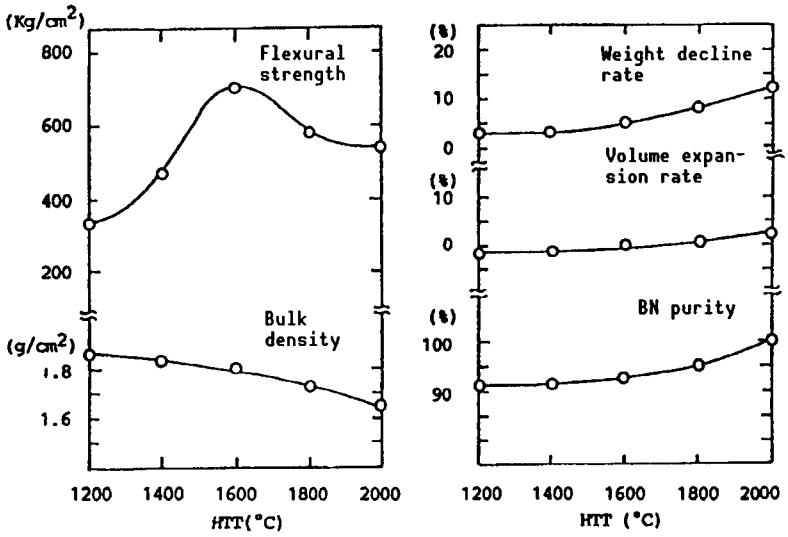


Figure 4. Effects of Temperature in Heat Treatment

## 4.2 Properties of Atmospheric Pressure Sintered Compact

The properties of BN compacts sintered under atmospheric pressure have been found to be affected by the kinds of starting material powder, the material refining, and compositional adjustment and sintering temperature. Figure 4 shows the typical example of the properties. The data in the figure were obtained using sintered BN compacts, which were produced using the pulverized powder whose properties are given in Table 2. The compacts sintered at 1,600°C displayed the highest flexural strength. The compacts had fairly low material purity and still contained impurities. Sintering at still higher temperatures improved purity at the expense of a slight decline in the strength. In many cases, the pulverized BN powder still contains impurities, mainly oxygen and much boron. They are considered to exist in the form of amorphous BOx and B–N–O–system intermediate products. The compacts sintered at 1,600°C contained boron oxide and an ambiguous crystal phase, and they gradually disappeared as sintering temperature was increased further, and disappeared almost completely when the temperature reached 2,000°C. This led us to believe that the decline in the sintered compact's weight above 1,600°C resulted from the evaporation of boron oxide and the amorphous phase, contributing to an improvement of compact purity. When sintered, pulverized BN powder causes a light bubble in the sintered compact due to the heat involved. But the degree of bubble is very small compared to using nonpulverized powder. When nonpulverized BN powder was sintered under the same condition, the volume of the sintered compact increased by about 10 percent due to free expansion. All the BN compacts sintered using the BN powder, which was subjected to a 48-hour pulverization at a temperature of 2,000°C, had a purity higher than 99 percent and they also displayed fairly good mechanical characteristics. Table 3 shows the typical properties of these compacts sintered under atmospheric pressure at 2,000°C. The compacts produced using high-purity, well-crystallized BN-a powder displayed a comparatively high mechanical strength.

A major feature of the BN compacts sintered using our atmospheric sintering method is the high material purity. The sintered compacts thus produced have a porous structure in which BN crystal grains in the plane like configuration are oriented in random three-dimensional ways to present a structure like a cardhouse. This is another feature of atmospheric pressure sintered BN compacts. In hot press sintered compacts, BN grains have a crystal structure in which B grains appear in contact with N grains, whereas in atmospheric pressure sintered counterparts, the B and N grains are bonded together, giving a structural continuity in molecular level. Even if material density is not so high, BN sintered compacts exhibit comparatively good mechanical properties, and it is believed that the firm and stable cardhouse structure is responsible for this. Pulverized BN powder contains a comparatively high level of oxygen, and during sintering such oxygen reacts with the material powder to produce boron oxide and other byproducts. It is well known that boron oxide acts as a catalyst that promotes crystallization in BN compact. However, not much is known about the effects that the oxygen, introduced into BN powder in the process of mechanochemical treatment of the powder, could give to the results of atmospheric pressure sintering.

Table 3. Properties of Atmospheric Pressure Sintered BN Compact

| Starting material | Atmospheric pressure sintering BN-a | BN-b | Hot press[1] |
|---|---|---|---|
| BN purity (%) | 99.6 | 99.9 | 99.0 |
| Density ($g/cm^3$) | 1.50 | 1.64 | 1.85 |
| Flexural strength (MPa) | 22 | 38 | 34 |
| Hardness (ShorD) | 27 | 24 | 14 |
| Thermal conductivity ($W/m \cdot k$) | 37 | 37 | 63 |
| Electrical resistance ($\Omega \cdot cm$) | $>10^{15}$ | $>10^{15}$ | $>10^{15}$ |

1) Temperature: 2,000°C, pressure: 15 MPa

## 5. Epilogue

Use of h-BN ceramic powder in producing various kinds of crucibles, protective pipes, heat radiators, and other ceramic products has been increasing in recent years. As a new method in addition to the conventional hot press method, this author's group has developed an atmosphere sintering method involving the use of pulverized BN powder to produce BN sintered compacts. Our method requires no sintered compact machining, contributing to promotion of the compact's use. The BN compacts produced using the atmosphere sintering method are beginning to be used commercially. So far in this section, I have described the atmospheric sintering method involving the use of pulverized BN powder, hoping that this article could attract a stronger interest in the use of cubic boron nitride as a ceramic material.

**High-Performance Sintered β-SiAlON Compact**

916C0027C Tokyo KENKYU KOENKAI YOSHISHU in Japanese 19 Mar 91 pp 33-37

[Article by Kazushi Kishi, Government Industrial Research Institute, Kyushu: "Production of High-Performance Sintered β-SiAlON Compact Using Aluminum Alkoxide"]

[Text] **1. Introduction**

The sintered β-SiAlON compact's superb performance in high-temperature strength, antioxidation capability, and anticorrosion ability makes it popular along with silicon nitride ($Si_3N_4$) and silicon carbide (SiC) compacts to produce high-temperature-use structural materials like one used in gas turbines. β-SiAlON is a solid solution in which the Si in β-$Si_3N_4$ was displaced with Al and the N with O, and is expressed as $Si_{6-z}Al_zO_zN_{8-z}$ in chemical formula. The volumes of Al and O within the solid solution, represented with z in the formula, are in the range between 0~4.2. Commonly, sintered β-SiAlON compact is being produced by mixing the powder of $Si_3N_4$ and alumina ($Al_2O_3$) or $Si_3N_4$, $Al_2O_3$ and aluminum nitride (AlN), or $Si_3N_4$ and silica ($SiO_2$) in appropriate mixing ratios and sintering the molded compacts.

The sintered β-SiAlON compact manufactured by the conventional method using $Al_2O_3$ powder as the main ingredient has a low mechanical strength ranging from 30~60 kg/mm$^2$. This compares with the strength of 80~120 kgf/mm$^2$ in sintered $Si_3N_4$ compacts, which were produced by adding magnesia (MgO) or $Al_2O_3$ and $Y_2O_3$ as sinter-promotion agents, or with the strength of sintered SiC compacts ranging from 60~90 kgf/mm$^2$ produced using B and C as sinter-promotion additives. The principal reason for the comparatively low strength of β-SiAlON is traced to the presence of a structural nonuniformity within the compact due to the presence of clusters of coarse, large-diameter powder grains and pores.

Synthesis of sintered β-SiAlON compacts goes through the following processes. At first, a reaction occurs between $Si_3N_4$ and $Al_2O_3$ powders to generate a low-melting-point X phase, and the synthesis of β-SiAlON and the sintering process proceed assisted by the liquid phase of the melted X phase. The pores and the clusters of coarse, large-diameter grains are believed to be produced due to the nonuniformity in the distribution of the liquid phase; i.e., where the liquid phase is scarce, the pores and portions of insufficient reaction

appear, and where the phase exists is abundant, the clusters of coarse, large-diameter grains appear as a result of abnormal growth of the grains.

If structural uniformity in sintered compacts could be improved, the strength in centered $\beta$-SiAlON compacts could be increased. Consequently, it is very important to improve uniformity in the distribution of $Al_2O_3$ within material powder.

A method to scatter $Al_2O_3$ within $Si_3N_4$ material powder without using it in powder form involves using an $Al_2O_3$-source solution, into which $Si_3N_4$ powder is scattered to obtain a compound material powder by having the $Al_2O_3$ content precipitate on the surface of $Si_3N_4$ powder grains during the drying and calcination process.

Metal alkoxide reacts well with a functional group such as a hydroxyl group on the surface of ceramic material powder grains, and this makes it widely used in heating the surface quality of the grains and in improving the material powder uniformity within sintered ceramic compacts. Aluminum alkoxide {$Al(OR)_3$}, too, is believed to form a reaction layer on the surface of $Si_3N_4$ powder grains as a result of a reaction with the hydroxyl group on the surface. Consequently, it is believed that the uniform scattering of the material powder can be improved by treating $Si_3N_4$ powder with $Al(OR)_3$ to improve the surface quality of the powder grains. $Al(OR)_3$ can be turned into $Al_2O_3$ easily by baking the chemical-containing compact, or baking after a hydrolysis process. This could make it possible to produce a compound $Si_3N_4$ powder in which the surface of powder grains is covered with a film of $Al_2O_3$ by calcinating the mixture of the powders of these chemicals, or calcinating after a hydrolysis process.

In the following, the results of this author's effort to produce sintered $\beta$-SiAlON compacts using compound $Si_3N_4$-$Al_2O_3$ material powder, which was prepared using the technique described above, will be described. The results of measurements to study the mechanical strength and antioxidation capability of the sintered compacts will also be described.

## 2. Experiment Method

### 2.1 Production of Sintered Compacts

Using aluminum isopropoxide <$Al(Oi-Pr)_3$> and $Si_3N_4$ powder and the following three procedures, compound $Si_3N_4$-$Al_2O_3$ material powder was synthesized, and using the powder and a carbon die having a minor diameter of 30 mm square, sintered compacts were produced by hot pressing the powder under a pressure of 300 kg/cm$^2$ and a temperature of 1,850°C for one hour. The compound powder contained no low-melting point X phase and had a z value of 0.5. After studying each of these compacts for bulk density, synthesized phase, and crystal structure, another set of sintered compacts using $\alpha$-$Al_2O_3$ powder as the material was produced under the same sinter conditions, and a comparison was made between the two sets of compacts in properties.

Procedure I: $Al(Oi-Pr)_3$ was dissolved into dehydrated n-hexane ($C_6H_{14}$) and the solution was filtered to remove aluminum hydroxide ($Al(OH)_3$) floating within the $Al(Oi-Pr)_3$ solution. The filtered out $Al(OH)_3$ was calcinated and its weight was measured, and the volume of $Al(Oi-Pr)_3$ in the $Al(OH)_3$-removed solution was corrected accordingly. Then $\alpha$-$Si_3N_4$ powder was added to this solution at a weight ratio of $Al(Oi-Pr)_3:Si_3N_4$ = 28.41:71.59 ($Al_2O_3:Si_3N_4$ = 9.01:90.99), and together with $Si_3N_4$ balls the solution was mixed for 20 hours. After the mixing was completed, the suspension was spray-dried and compound $Si_3N_4$-$Al_2O_3$ powder was produced by calcinating the dried powder in an air atmosphere for two hours.

Procedure II: $\alpha$-$Si_3N_4$ powder was added to the $Al(Oi-Pr)_3/n-C_6H_{14}$ solution prepared using the same technique described in Procedure I, and after mixing, the solution was hydrolyzed by introducing distilled water. The pH value of the hydrolyzed solution was adjusted to stand between 2 and 4 by adding diluted hydrochloric acid, and then it was stirred for 24 hours to deflocculate. The suspension obtained after deflocculation was spray-dried in the same way as in Procedure I and the compound powder was obtained by calcinating the suspension.

Procedure III: $Al(Oi-Pr)_3$ was added to 80°C distilled water and the fluid was hydrolyzed. After cooling the hydrolyzed solution, the pH value of it was adjusted to 3 by adding diluted hydrochloric acid, and after stirring for 24 hours the solution was deflocculated to obtain aluminum hydroxide sol. After the sol was filtered to remove coarse agglomerates of aluminum hydroxide, $\alpha$-$Si_3N_4$ powder was added at a ratio of $Al_2O_3:Si_3N_4$ = 9.01:90.99 and mixed together with $Si_3N_4$ balls for 24 hours. After the mixing was completed, the suspension was spray-dried and was calcinated in a 600°C air atmosphere for two hours to obtain the compound powder.

Figure 1 shows the outline of the methods for producing compound $Si_3N_4$-$Al_2O_3$ powder.

## 2.2 Strength of Sintered Compact

The samples for the measurement of flexural strength, with each measuring about 3 x 3 x 30 mm, were prepared by cutting out six chunks of ceramics from each of the sintered compacts produced using the above methods, by surface grinding using a #600 diamond grinding wheel, and by rounding the surface corners using #800 SiC paper. Measurement of flexural strength was taken using a 20-mm span, three-point flexural strength tester at a cross-head speed of 0.5 mm/min.

First, the test samples prepared from the sintered compacts produced using the Procedure I method were subjected to a heat treatment involving heating from 0.5~10 hours in a 1,200°C air atmosphere inside a kanthal super furnace to study the change of flexural strength as a result of the treatment. In this measurement, three to four test samples were prepared for each of the production methods.

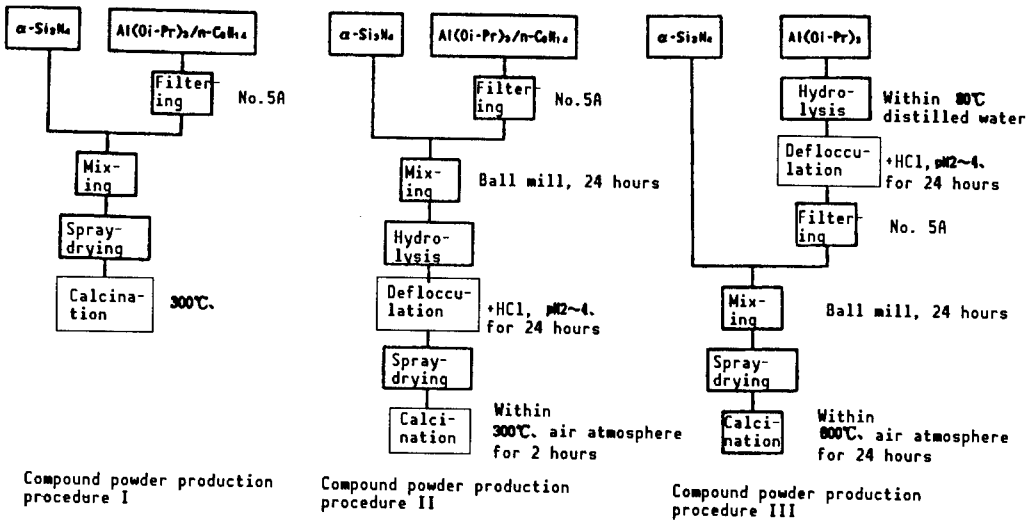


Figure 1. Outline of the Three Compound Powder Production Methods

After the flexural strength, microscopic observation of the broken samples was made using an optical microscope and a scanning electron microscope (SEM).

### 2.3 Antioxidation Capability of Sintered Compact

In the experiment to test the antioxidation capability of sintered compacts, compacts produced using the Procedure I method were used. As comparison samples, $Y_2O_3$–added $\beta$–SiAlON HNC–10 manufactured by Hitachi Metals, Ltd., was used. In the experiment, 3 x 3 x 30 mm test samples were prepared by grinding the surface using a #600 diamond grinding wheel.

The samples ranging in number from three to four were arranged on alumina plates having platinum wires laid on them, and the samples were oxidized by being heated inside a kanthal super furnace at 1,200°C and 1,400°C within an air atmosphere for 25, 50, 100, and 200 hours, respectively. The oxidized samples were measured for changes in weight and flexural strength, and the surface condition and the broken faces were examined using an optical microscope and an SEM.

## 3. Results and Discussion

### 3.1 Strength of sintered Compact

Table 1 gives the bulk densities, synthesized phases, and the flexural strength of the three types of sintered compacts produced using methods I, II, and III and a compact sintered using $\alpha$–$Al_2O_3$ powder.

These sintered compacts had high densities with each having a water absorption rate of less than 0.01 percent. The type I and II compacts had a bulk density of 3.14 g/cm$^3$ each, and the type III compact had a slightly smaller value at 3.12 g/cm$^3$. All these three types of sintered compacts had a crystal phase composed of $\beta$–SiAlON and smaller amounts of O'SiAlON.

Table 1. Bulk Densities, Synthesized Phases, and Flexural Strength in Four Different Types of Sintered Compacts

| Sample type | Density ($g/cm^3$) | Synthesized phase | $\frac{O'(200)}{\beta(110)+O'(200)}$ | Flexural strength | | |
|---|---|---|---|---|---|---|
| | | | | Mean value | Maximum value | Minimum value |
| I | 3.14 | $\beta$ + O' | 0.13 | 84.9 | 99.0 | 80.8 |
| II | 3.14 | $\beta$ + O' | 0.14 | 88.1 | 95.6 | 79.1 |
| III | 3.12 | $\beta$ + O' | 0.22 | 80.4 | 90.2 | 72.0 |
| $Al_2O_3$ | 3.14 | $\beta$ + $\alpha$ | — | 49.4 | 54.2 | 45.6 |

$\beta$ : $\beta$–SiAlON
O': O'SiAlON
$\alpha$ : $\alpha$–$Si_3N_4$

The X-ray relative strength (O'(200)/O'(200)+$\beta$(110)) of O'SiAlON stood at 0.13 in type I and II compacts and at a slightly larger value of 0.22 in the type III compacts. This indicates that by mixing $Si_3N_4$ powder within a solution, the powder underwent a hydrolysis, and it is believed that the smaller bulk density of type III compacts is attributed to the larger volume of synthesized O'SiAlON. However, all these three types of compacts displayed flexural strength far larger than 80 $kgf/mm^2$, and this is higher than some 50 $kgf/mm^2$ in the $Al2O_3$ compacts.

Optical microscope observation found that all three types of compacts had uniform material structure different from the $Al_2O_3$–sintered compacts that contained black nonuniform spots. The uniform material structure was made up of the crystal grains of $\beta$–SiAlON with their diameter ranging from 0.5~1 $\mu$m and a small amount of a grain boundary phase structure, most of which was removed by an anticorrosion treatment given to the compacts, whereas within the $Al_2O_3$ compacts nonuniform portions containing coarse, and irregular-size grains were found. Even the distribution of the grain boundary phase structure displayed a uniform pattern. From these results it can be said that all three sintered compact production methods are useful in producing uniform and high-strength sintered $\beta$–SiAlON compacts.

In a tensile break test, it has been found that the coarse-structured nonuniform portions in sintered $Al_2O_3$ compacts were responsible for the destruction of the compacts, whereas in the types I, II, and III compacts the machining scars made on the surface of samples during the grinding process were responsible. From this result, it can be said that removal of the coarse-structured nonuniform portions from the three types of sintered compacts contributed chiefly to increasing the strength in them.

These sintered compacts have a comparatively small $K_{IC}$ value ranging from 3.0~3.3 $MNm^{-3/2}$, and due to this it is believed that their strength is more susceptible to the machining scars.

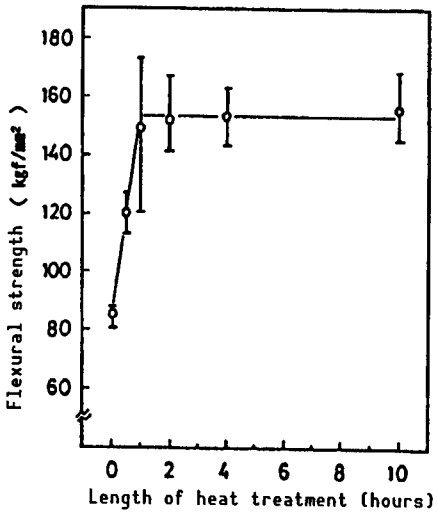


Figure 2. Change of Strength in Type I Sintered Compacts After They Were Given an Additional Heat Treatment

Despite this, all the compacts have a strength higher than 80 kgf/mm$^2$, and some showed a maximum strength reaching about 100 kgf/mm$^2$. It is believed that if the machining scars can be reduced, the strength would increase further.

Figure 2 shows the change of strength in the test samples of the type I sintered compacts after they were given an additional heat treatment. After one-half hour of treatment, the strength increased to about 120 kgf/mm$^2$; after one hour of treatment, to about 150 kgf/mm$^2$; and after that, almost no improvement, with the figure unchanged after 10 hours of heat treatment. Those compacts subjected to a heat treatment for more than one hour were covered with a uniform oxide film. No cracks were found within the film, except for the machining scars that were still seen clearly through the film. In these heat-treated samples, it is believed that the improvement in strength was achieved as a result of obscuring the surface-side ends of the cracks caused by the machining and the oxide film blanketing the samples, contributing to reducing the adverse effects of machining scars.

In some of the tested samples, break was caused apparently after semicircular cracks developing perpendicularly to the depth direction of machining scars. Even in many other samples in which the cause of break was not pinpointed so clearly, it was found that break started at a point near clearly visible machining scars. From this result, it is believed that the strength of sintered compacts can be improved further if the scars can be made smaller and uniform.

### 3.2 Antioxidation Capability of Sintered Compact

Figure 3 shows the relationship between the length of oxidation time and the progress in oxidation in the test samples of the two types of sintered compacts. In all these samples, an increase of weight was observed when oxidation progressed.

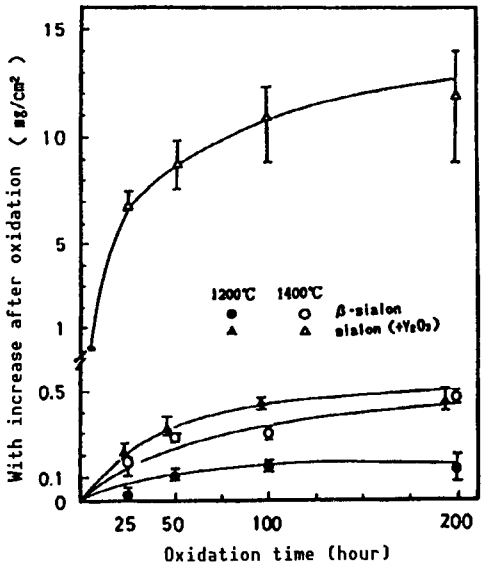


Figure 3. Increase of Weight in Two Types of Sintered Compact Samples After Oxidation

In the samples of the type I sintered compacts, the weight increase was very small compared to Y-SiAlON; after 200 hours of an oxidation process under a temperature of 1,200°C the increase was only about 0.1 mg/cm$^2$, and even when the temperature was raised to 1,400°C the increase stood at about 0.4 mg/cm$^2$. In Y-SiAlON, which was oxidized at 1,200°C, the weight continued to increase up to 50 hours of oxidation with the increase reaching about 0.35 mg/cm$^2$. After that the rate of increase dampened with the weight increase, reaching about 0.4 mg/cm$^2$ at 200 hours of oxidation. At a temperature of 1,400°C, the weight increase reached about 7 mg/cm$^2$ at 25 hours of oxidation, and about 11 mg/cm$^2$ at 200 hours.

In the test samples of the type I sintered compacts, the thickness of oxide film on the surface continued to grow gradually as oxidation time increased. The oxide film had smooth surface texture and even after 200 hours of oxidation the machining scars could be seen clearly through the film. There were no test samples in which either bubbles or cracks were seen within the film. The thickness of the oxide film stood at about 3 $\mu$m when the samples were subjected to a 200-hour oxidation of 1,200°C, and this increased to about 8 $\mu$m when the temperature was increased to 1,400°C. The boundary between the film and the test sample was not so clear, indicating that the film was bonded to the sample firmly, and thus, the film is working as an effective protector of the compact.

In the Y-SiAlON oxidized at 1,200°C, bubbles were formed within the oxide film in the early stage of oxidation, and the scale of bubbles continued to increase until 50 hours of oxidation. Judging from the result that a smooth-surfaced oxide film grew to a thickness ranging from 100~200 $\mu$m after an oxidation of 100~200 hours, it can be considered that once an oxide film has grown to the degree of enveloping the test sample the growth speed dampens a little.

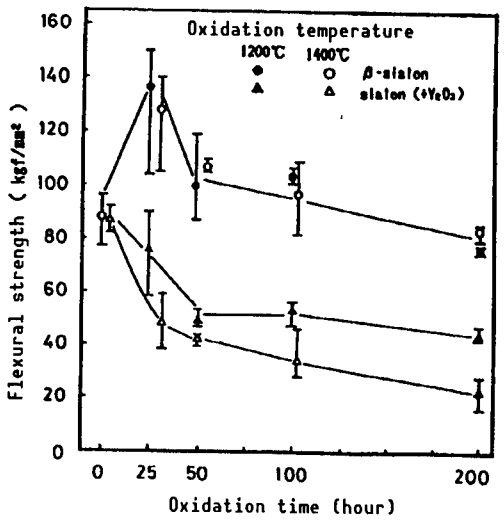


Figure 4. Change of Flexural Strength in Two Types of Oxidized Sintered Compact Samples

Although the weight increase in Y-SiAlON samples was larger than the type I sintered compact samples, many of the cracks and irregular crystal structures were found within the oxide film, and due to this the usefulness of the film as a protective layer is considered to be far smaller than the film in the type I samples. In fact, in Y-SiAlON samples that were oxidized for 25 hours at 1,400°C, it was found that oxide film up to about 100 $\mu$m thick was peeling off the samples' surface. It was also observed that when the oxide film continued to grow, cracks developed on the surface of Y-SiAlON samples at a depth ranging from about 150~200 $\mu$m, and oxidation progressed deeper into the samples while the oxide film peeled off the cracked samples' surface. From this, it can be said that at that temperature, the oxide film has little effectiveness as a protective film.

Figure 4 shows the changes in flexural strength in the two types of sintered compacts. The type I sintered compacts' flexural strength was almost unchanged at 1,200°C and 1,400°C. In the compacts, the strength increased to about 140 kgf/mm$^2$ after 25 hours of oxidation, and after this the strength gradually declined to reach about 80 kgf/mm$^2$ after 200 hours of oxidation, nearly the same strength as that of nonoxidized samples. On the other hand, in Y-SiAlON samples oxidized at 1,200°C, flexural strength decreased from about 90 kgf/mm$^2$ in nonoxidized samples to about 80 kgf/mm$^2$ after 25 hours of oxidation, to about 50 kgf/mm$^2$ after 50 hours. After that the strength almost stabilized. At 1,400°C, the strength declined to about 50 kgf/mm$^2$ after 25 hours of oxidation, and declined further to about 20 kgf/mm$^2$ after 200 hours of oxidation.

In the type I sintered compacts, break started from the concave part believed to have been created by the machining in the nonoxidized samples and the samples oxidized for 25 hours at 1,200°C. In all other samples, break started from the boundary between the oxide film and the sample. In these samples, no bubbles or nonuniform crystal structures were found. This indicates that break was caused as a result of stresses appearing between the oxide film and the sample.

After 400 hours of oxidation at 1,400°C, the type I sintered compact samples had a flexural strength of 78.4 $kgf/mm^2$, almost the same value as that of nonoxidized samples or ones oxidized for 200 hours. The compact's samples, in which an oxidation was carried out at 1,400°C for 100 hours and then the oxide film was removed using a 6 $\mu m$ diamond disk grinder, had a flexural strength of 130 $kgf/mm^2$, a value higher than that of nonoxidized samples. From these results, it can be considered that the reason for the decline of flexural strength in the oxidized samples can be attributed to stresses appearing in the boundary between the oxide film and the sample.

In all the Y-SiAlON samples oxidized at 1,200°C, break started from the bubble sections within the oxide film. Decline of flexural strength in these samples up to the oxidation time of 50 hours is believed to have been caused by the formation of bubbles within the oxide film and continued growth of them. After an oxidation of 100 hours, the flexural strength almost stabilized, and this is believed to have resulted from ceased growth of the bubbles after that time and from increased thickness of the oxide film. In the Y-SiAlON samples oxidized at 1,400°C, the breaking point could not be pinpointed. However, it is believed that break started from the portion having the most conspicuous machining scars as a result of peeling of the oxide film. Considering the fact that the peeling worsened as oxidation time increased, it is believed that the flexural strength of Y-SiAlON samples declined in proportion to the length of oxidation time. From these results and observations, it is believed that using sintered Y-SiAlON compacts in 1,400°C air atmosphere is virtually impossible.

## 4. Epilogue

The flexural strength and antioxidation capability of sintered $\beta$-SiAlON compacts, which were produced using compound $Si_3N_4$-$Al_2O_3$ powder synthesized from $Si_3N_4$ and $Al(Oi\text{-}Pr)_3$ as starting materials, were studied.

The compound powder having a z composition of 0.5 was produced using three different methods, and the sintered compacts were produced using the hot press method. In producing the compound powder the three methods involved 1) mixing of $Si_3N_4$ powder with $Al(Oi\text{-}Pr)_3$ solution and calcination of the mixture after it was spray-dried; 2) mixing of $Si_3N_4$ powder with $Al(Oi\text{-}Pr)_3$ solution, followed by the mixture's hydrolysis, deflocculation, and calcination of the spray-dried powder; and 3) hydrolysis of $Al(Oi\text{-}Pr)_3$ solution, followed by mixing of $Si_3N_4$ powder with aluminum hydroxide sol solution, which was obtained by deflocculation of the hydrolyzed product and then calcination of the spray-dried powder.

The sintered compacts produced using the compound powder were made up of $\beta$-SiAlON and a small amount of O'SiAlON. In the sintered compacts produced using the type III compound powder, the amount of O'SiAlON was slightly higher than other compacts. This resulted from the $Si_3N_4$ powder's hydrolysis while the powder was mixed with water. However, all the sintered compacts produced using compound $Si_3N_4$-$Al_2O_3$ powder had a uniform crystal structure composed of $\beta$-SiAlON ranging from 0.5~1 $\mu m$ in crystallized grain diameter and a small amount of grain boundary phase. No coarse, nonuniform structure, which was found in sintered $Al_2O_3$ compacts, was observed.

All the sintered compacts produced using the compound powder exhibited a flexural strength ranging from 80~90 $kgf/mm^2$. This compared to a strength of about 50 $kgf/mm^2$ in the sintered $Al_2O_3$ compacts. The higher strength was achieved as a result of improved uniformity in the crystal structure in the sintered compacts produced using the compound powder. In all these compacts, break in the test samples started at the machining scars on the surface.

Based on the finding that the strength of a uniform structured sintered compact is affected greatly by the presence of machining scars on the surface, attempt was made to increase the strength by providing an additional heat treatment to the test samples of sintered compacts. In the samples produced using the type I composite powder, the flexural strength was improved to about 150 $kgf/mm^2$ by giving a heat treatment in a 1,200°C air atmosphere for one hour. The strength was unchanged up to 10 hours of heating. On the other hand, the antioxidation capability of the sintered $\beta$-SiAlON produced using compound $Si_3N_4$-$Al_2O_3$ powder was compared with that of a sintered SiAlON compact produced by adding commonly available $Y_2O_3$. The increased weight in the sintered compacts produced using the compound powder was only about 0.4 $mg/cm^2$ after a heat treatment of 200 hours at 1,400°C, and their strength of about 80 kgf/mm2 after 400 hours of oxidation at 1,400°C was almost unchanged from the strength of the nonoxidized compacts. The uniform oxide film formed on the surface contained no bubbles, cracks, or nonuniform crystal structures. In the $Y_2O_3$-containing sintered compacts, a thick oxide film containing bubbles and cracks formed on their surface at an oxidation temperature of 1,200°C, and the compacts' strength deteriorated to half that of nonoxidized compacts. At 1,400°C, a massive peeling off of the oxide film, having grown to a thickness ranging from 150~200 $\mu m$, occurred and the strength of the oxidized compacts decreased to less than one-fourth of the nonoxidized counterparts.

**Ceramic Film Coating Using Sputtering Method**

916C0027D Tokyo KENKYU KOENKAI YOSHISHU in Japanese 19 Mar 91 pp 39-44

[Article by Kaoru Shibata, Government Industrial Research Institute, Kyushu: "Ceramic Film Coating Using Sputtering Method"]

[Text] **1. Introduction**

The use of ceramics in coating the surface of metal and other kinds of materials by taking advantage of its fine antiwear, antiheat, and anticorrosion capabilities dates back to the first use of porcelain enamel to coat surfaces. Since then, the kinds of materials and methods used to form ceramic film have increased to meet diversified needs in industrial applications, and today, a great number of combinations of film materials are available. Methods for forming ceramic film, include the PVD, CVD, flame coating, and liquid phase methods. The PVD method is subdivided into the vapor deposition method, sputtering method, and ion plating method. In the rest of this article, discussion will concentrate on the sputtering method.

When the surface of a solid body is bombarded with accelerated ions, atoms, and ions are driven out from the surface as a result of the oncoming speeding ions exchanging the momentum with the atoms on the body surface. This phenomenon is known as sputtering. In the sputtering method, a ceramic film is formed by causing a transfer of a material through this phenomenon. In practical application, the precipitation of the coating film is realized by causing plasma ions to collide at a high speed with a negative potential target material (Figure 1). When the target is an electrically nonconductive material, high frequencies are used for sputtering. Argon is commonly used to produce the plasma. The advantages of the sputtering method are: 1) a high adhesion power of the precipitated film; 2) capability to form a film having a high melting temperature; 3) availability of a uniform and large area film; 4) ease in controlling film material composition; 5) capability to form a film without heating the substrate; and 6) capability to form a compound material film. Considering the fact that many of the ceramic-based materials used to form the film have high melting temperatures, the sputtering method is a suitable one. The disadvantages of the sputtering method are: 1) slowness in having the film precipitate, and 2) a comparatively high level of sputtering gas content within the precipitated coating film. However, the development of a magnetron sputtering system has made these disadvantages less problematical.

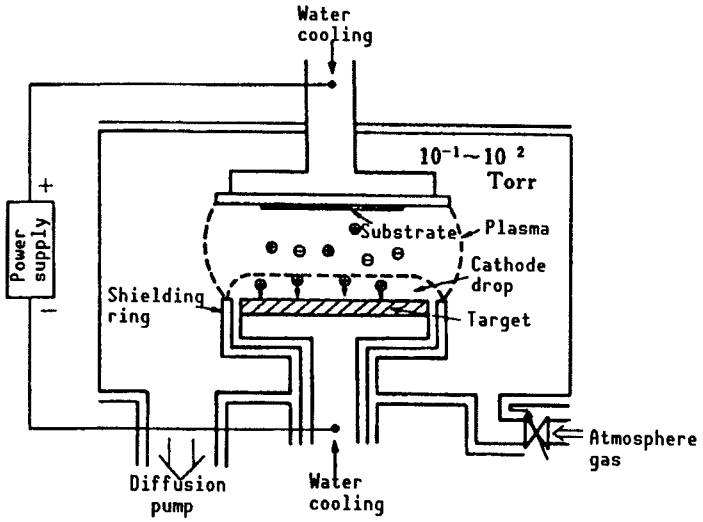


Figure 1. Outline of a Sputtering System

Ceramic films using the sputtering method for electronics field applications are TaN film used in manufacturing thin-film resistors, and ZnO, $LiNbO_3$, and $SiO_2$ films, all used as piezoelectric materials. Many kinds of thin ceramic films have been synthesized for structural material applications. $MoS_2$ film is being used in some U.S. satellites as solid lubrication film by being sputtered to the antifriction bearings. TiN film is being used by some European tool makers by being sputtered to high-speed steel tools using magnetron sputtering systems.

Demand for boron nitride (BN) has sharply increased in recent years because of the fine ceramics' good heat radiating and electrical insulating capabilities. However, it has been found recently that boron nitride carbon (BNC) has a better thermal and chemical stability and electrical insulating capability than BN, and it is drawing increasing attention as a new type of high-temperature-application engineering ceramics. Table 1 gives the values representing the properties of these two types of ceramics. BNC has a specific resistance value a little lower than BN up to around 1,000°C. However, at 1,400°C the resistance value shoots up to a level one digit higher than that of BN, and at 1,800°C to a level more than three digits higher. At 2,000°C, BNC still maintains a resistance value of $2 \times 10^4 \Omega \cdot cm$. In terms of thermal conductivity, BNC has a larger value than BN, and the former has a thermal expansion coefficient of about one digit lower than BN. BNC ceramics exhibits a good temperature stability up to about 3,000°C a nitrogen environment, and even in air atmosphere it is stable up to about 1,500°C, displaying good anti-oxidation capability.

Considering the superior capabilities of BNC ceramics, it is expected that the ceramics would find wide-ranging applications as an engineering material, an electronic insulator, and a protective film material for use in high-temperature environments. However, research in synthesizing BNC ceramics and evaluating its characteristics has started only recently. Particularly, research in synthesizing a thin BNC film and evaluating its characteristics

Table 1. Values Representing the Properties of BN and BNC Ceramics

| *Property* | *Temperature* (°C) | *Boron nitride BN* | *Boron carbonitride BNC* |
|---|---|---|---|
| *Resistivity* ($\Omega$ cm) | 20 | $>10^{13}$ | $>10^{13}$ |
| | 500 | $1.2 \times 10^{11}$ | $2 \times 10^{10}$ |
| | 800 | — | $3 \times 10^{7}$ |
| | 1000 | $1.1 \times 10^{7}$ | $5 \times 10^{6}$ |
| | 1200 | $1.8 \times 10^{5}$ | $3 \times 10^{6}$ |
| | 1400 | $5 \times 10^{4}$ | $5 \times 10^{5}$ |
| | 1600 | $1 \times 10^{3}$ | $3 \times 10^{4}$ |
| | 1800 | $2 \times 10^{1}$ | $2.5 \times 10^{4}$ |
| | 2000 | — | $2 \times 10^{4}$ |
| *Heat conductivity* ($W\,mK^{-1}$) | 350 | 9.31 | 27.0 |
| | 700 | 10.25 | 15.9 |
| | 1300 | 8.5 | 11.0 |
| | 1500 | 8.0 | 10.5 |
| *Thermal expansion coefficient* ($\times 10^{-6}\,K^{-1}$) | 10 - 1100 | — | — |
| | 20 - 2000 | 9.2 - 10.2 | 0.77 - 4.6 |

is very important to promote practical use of the ceramics. So far, only a small number of research papers have been published whose topics are confined to the chemical vapor deposition (CVD) synthesis method.

In an effort to develop a thin film having lubricating and antiwear capabilities, this author's research team has been conducting research to develop a compound material film by combining self-lubricating carbon and wear-resisting ceramics using the sputtering method. In the following sections I will discuss BNC film coating techniques using compound target materials composed of graphite and ceramics and two high-frequency magnetron sputtering methods.

## 2. Coating Method

Bulk BNC ceramics can be produced by sintering BN and boron carbide ($B_4C$) powder under a high-temperature and high-pressure environment. However, this author's team tried the coating using two kinds of compound material target and two different sputtering methods. One of the methods involved using a compound target composed of graphite and BN and the conventional sputtering method, and the other using a compound target consisting of graphite and $B_4C$ and the nitrogen reactive sputtering method.

### 2.1 Sputtering System

As a sputtering system, the commonly available high-frequency magnetron sputtering machine was used. Figure 2 shows the electrode arrangement in the machine. Two types of four-inch diameter targets were prepared by bonding a semicircular graphite disk and a same-shaped BN disk for the one target and a similar graphite disk and a semicircular $B_4C$ disk for the other target. As the material (substrate) on which the coating is applied, four 10 mm square glass

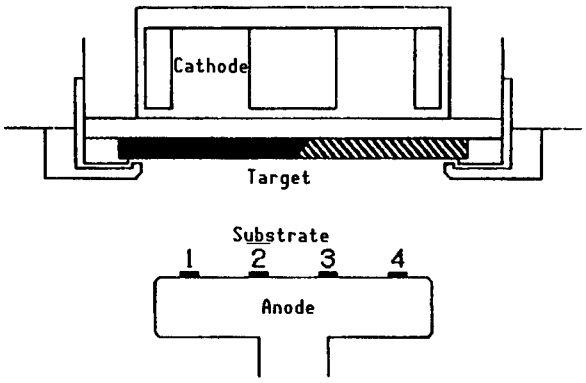


Figure 2. Electrode Arrangement in a High-Frequency Magnetron Sputtering Machine

plates with a thickness of 1 mm were used by setting on the substrate holders spaced equally for a simultaneous coating (Figure 2). The argon and nitrogen gas used in the sputtering had a purity of 99.999 percent and 99.99 percent, respectively.

### 2.2 Sputtering Using Compound Graphite/BN Target

First, the coating procedure involved conducting a preliminary sputtering by introducing argon gas into the $10^{-5}$Pa sputtering chamber up to the 1 Pa level and by applying 400 W high-frequency electric power for one hour. Then the sputtered samples were subjected to an additional process in which they were sputtered, for one set of samples, under a constant 400 W high-frequency electric power by shifting argon sputtering gas pressure to 0.3, 0.8, and to 5 Pa, and for another set of samples, under a constant 5 Pa, and for another set of samples, under a constant 5 Pa sputtering pressure by varying the power to 100, 200, and 400 W to complete the coating process.

The larger argon ion sputtering rate in the graphite than in the BN caused a faster coating speed in the substrates placed in the graphite target side. When sputtering pressure was increased, the coating speed in the substrates located in the BN side slowed down. When coating was carried out for 30 minutes under the high-frequency power strength of 400 W, a coating film thickness of about 1 $\mu$m was obtained at substrate 2.

### 2.3 Reactive Sputtering Using Compound Graphite/$B_4C$ Target

In carrying out a coating using the reactive sputtering method, a preliminary sputtering was conducted under the same condition as one described in section 2.1. After the preliminary process, coating was conducted under the fixed high-frequency power output of 400 W by varying the nitrogen gas sputtering pressure to 0.5, 1.0, and 1.5 Pa, and then by changing the nitrogen gas partial pressure to 0.1, 0.2, 0.6, and 1.0 Pa under a constant 1 Pa sputtering pressure.

Coating speed increased in proportion to the nitrogen gas sputtering pressure, and under the constant sputtering pressure in proportion to the nitrogen gas partial pressure. This tendency was observed particularly markedly in the substrates located in the graphite target side. When a coating was carried out for 15 minutes under the high-frequency power strength of 400 W and the nitrogen gas sputtering pressure of 1.5 Pa, the thickness of coating film on substrate 2 reached about 1 $\mu$m.

## 3. Characteristics of Coating Film

### 3.1 Coating Film Produced Using Compound Graphite/BN Target

#### (1) Photoelectron Spectrum

From the photoelectron spectrum observation, the coated film was found to consist of carbon, boron, nitrogen, oxygen, and argon. Because argon is believed to have mixed into the film in the process of coating or etching, and it is chemically inactive, argon is excluded from our discussion here.

Based on the integrated intensities of 1 s peaks in each of the chemical elements mentioned above, the compositions of these elements in each of the coated samples were obtained (Figures 3 and 4). As to the contents of carbon and boron in each of the substrates, when the contents of carbon increased those of boron decreased, and when carbon level decreased, boron level increased. This is only natural considering the positions of the substrates vis-a-vis the graphite and BN target materials. The nitrogen contents in these substrates showed an increase/decrease tendency similar to that of boron with the nitrogen level about one-half of boron. This is believed to have been caused by part of the nitrogen ions sputtering from the target having been exhausted out of the sputtering chamber. Regarding the composition on a single substrate, the contents of carbon increased in proportion to sputtering pressure, but those of boron and nitrogen decreased. This is, as described in section 2.2, because of a declining sputtering rate in the BN target when sputtering pressure increased. Considering that when the high-frequency power strength was reduced on the same substrate the contents of the carbon increased further and those of boron and nitrogen declined further, it suggests that when the power strength was lowered, the sputtering rate in BN decreased much more compared to the sputtering rate in the graphite.

The bonding energy level at 1 s peak was in the 189.7~190.2 eV range in boron, 285.1~284.1 eV range in carbon, and 399.7~398.6 eV range in nitrogen. Concerning the chemical shift of these values, study is continuing.

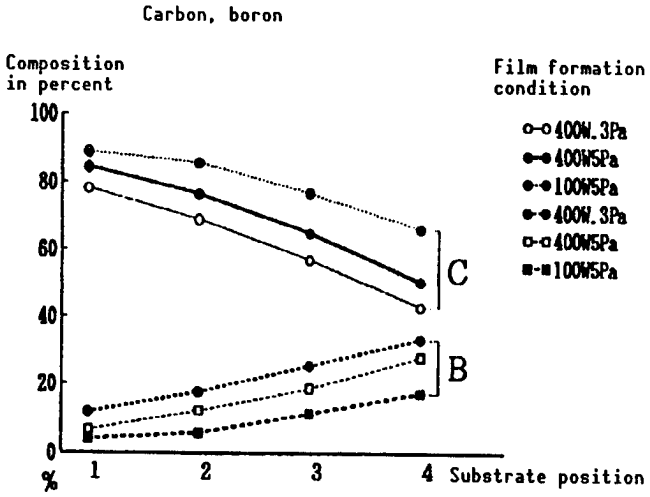


Figure 3. Chemical Element Compositions in BNC Films (1)

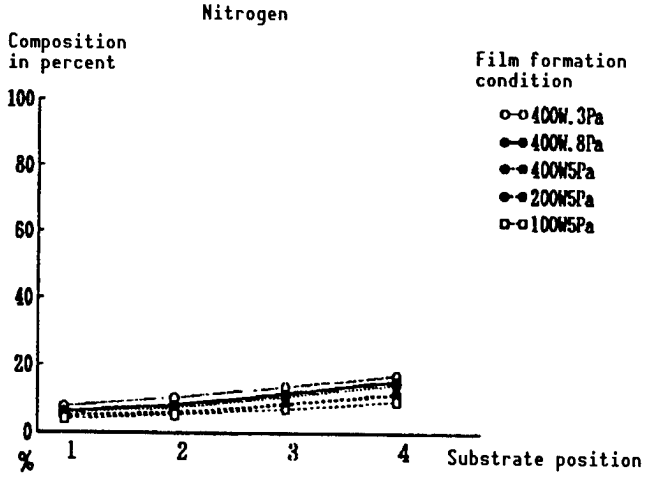


Figure 4. Chemical Element Compositions in BNC Films (2)

**(2) Infrared Absorption Spectrum**

Figure 5 shows the infrared absorption spectrum of a BNC sample film that was coated on a potassium bromide pellet under the high-frequency electric power strength of 400 W and the sputtering pressure of 0.8 Pa. In the figure, the absorption bands having peaks near 1,250 $cm^{-1}$ and 740 $cm^{-1}$ points are believed to have resulted from a shift caused by the stretching vibration of the B-N bonding (1,380 $cm^{-1}$) and the deformation vibration (800 $cm^{-1}$), respectively. The comparative broadness in the absorption bands indicates that the coated film is made up of an amorphous structure. That the absorption band strength increases as the substrate item number increases matches qualitatively with the results obtained from the observation of the photoelectron spectrum on the boron and nitrogen composition in the substrates.

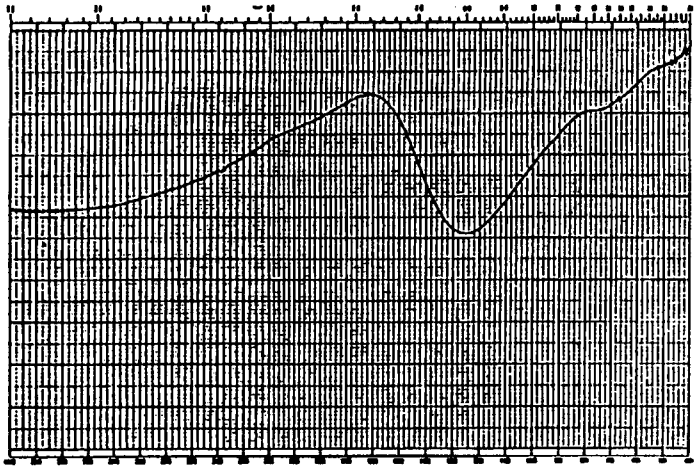

Figure 5. Infrared Absorption Spectrum in BNC Films

### 3.2 Coating Film Produced Using Compound Graphite/$B_4C$ Target

#### (1) Photoelectron Spectrum

A photoelectron spectrum analysis of a coating film produced using a compound graphite/$B_4C$ target found that the film was composed of carbon, boron, nitrogen, oxygen, and argon. However, for the same reason given in section 3.1, argon will be excluded from the discussion here.

Based on the integrated intensities of 1 s peaks in each of these chemical elements, the element compositions in the substrates coated under various film formation conditions were analyzed. As to nitrogen contents, they changed little when nitrogen sputtering pressure was changed between 0.5~1.5 Pa and when nitrogen partial pressure was varied by maintaining sputtering pressure at a constant level. Concerning the contents of carbon and boron, little change was observed in both of them when nitrogen sputtering pressure was changed between 0.5~1.5 Pa. However, carbon contents increased and boron contents decreased when nitrogen partial pressure was increased while maintaining sputtering pressure at a fixed level. This phenomenon can be attributed to the relative differences in the rate between the two materials in a nitrogen ion environment. This matches with the dependency of film coating speed on the nitrogen partial pressure level, as described in section 2.3.

The bonding energy level at the 1 s peaks were measured to range from 190.2~190.7 eV in boron, from 285.3~283.8 eV in carbon, and from 399.5~398.5 eV in nitrogen. Concerning the chemical shift of these values, study is continuing.

### (2) Infrared Absorption Spectrum

The infrared absorption spectrum of the coated films showed the absorption band peaks near 1,380 $cm^{-1}$ and 780 $cm^{-1}$ points, which are believed to have been caused because of the stretching vibration of B–N bonding and the deformation vibration. Another absorption band having a peak near 2,180 $cm^{-1}$ point is believed to have been caused by a multiple C–N bond vibration. The fact that these absorption bands have broad peaks indicates that the coated film is made up of an amorphous structure. The strength of the absorption bands matches qualitatively with the contents of the boron and nitrogen within the coated films, measured through the photoelectron spectrum analysis.

## 4. Epilogue

Using the conventional sputtering method or the reactive sputtering method, both involving the use of a compound material sputtering target, a substrate can be coated with a ceramic film composed of carbon, boron, nitrogen, and smaller amounts of oxygen and argon. The coating film has a high adhesive power with the substrate and a uniform smooth surface texture compound of an amorphous structure. The use of the two different sputtering methods produced two types of ceramic films that had different chemical bonding structures. However, many problems still remain that have to be solved concerning the formation of thin ceramic coating films. On the other hand, in the property evaluation of thin ceramic film, we could have measured only the hardness of the films we formed, and under the circumstances we must make efforts to expand evaluation items further. As described above, many problems concerning BNC film coating have yet to be solved. Despite the existence of unsolved problems concerning BNC film coating, I dared to introduce the results of our research on BNC film formation by recognizing the superior high-temperature characteristics and the capabilities of BNC ceramic film, which would make the film suitable as an electrical insulator as well as a protective film in high-temperature environments. I conclude this article hoping that what I have described can serve those who are engaged in research in similar fields.

**Sintering of Ti(C,N)-System Ceramics**

916C0027E Tokyo KENKYU KOENKAI YOSHISHU in Japanese 19 Mar 91 pp 45-50

[Article by Tadahiko Watanabe, et al., Government Industrial Research Institute, Kyushu: "Sintering of Ti(C,N)-System Ceramics and Its Characteristics"]

[Text] **1. Introduction**

Steel including carbon steel has contributed to the development of modern industry. In the boring and rough cutting of carbon steel material, either WC-Co cemented carbide tools or coated WC-Co cemented carbide tools are being used, and in finishing cutting TiN-system cermet tools are being used. TiN-system cermet tools have a cutting speed ranging from 200~250 m per minute, and effort is being made to develop a tool having a faster cutting and a longer service life.

In our research, we tried to produce ($Ti(C_{0.5}, N_{0.5})$-$Cr_3C_2$-system ceramics by sintering $Ti(C_{0.5}, N_{0.5})$ material powder containing $TiB_2$ and $Cr_3C_2$ as sinter promotion agents in a vacuum environment. Using these ceramics, we measured the cutting characteristics when they are used in finishing cutting tools. In the following, $Ti(C_{0.5}, N_{0.5})$ will be referred to simply as Ti(C,N).

**2. Experiment Method**

Table 1 gives the chemical composition of the material powders used in producing Ti(C,N)-$TiB_2$-system ceramics, and Table 2 gives the chemical composition in Ti(C,N)-$Cr_3C_2$-system ceramics.

The material powders were prepared by mixing them in an agitator for 1.2 ks. The mixture was press-molded using a die after it was granulated, followed by a 300 $MN/m^2$ cold isostatic pressing (CIP) mold process. The molded compacts were sintered at different temperatures in a vacuum environment for 5.4 ks.

The sintered compacts were studied in porosity, average diameter of Ti(C,N) grains, transverse rupture strength, Vickers hardness, fracture toughness, crystal structure, and composition. The porosity and the average diameter of Ti(C,N) grains were obtained by taking the crystal structure photos of the

Table 1. Chemical Composition and Grain Size of Raw Powder Materials

| No. | Raw material | Chemical composition and content (wt%) | Grain size ($\mu$m) |
|---|---|---|---|
| 1 | $Ti(C_{0.5},N_{0.5})$ | FC(0.05),Fe(0.08),$O_2$(0.62),W(7.0),Co(0.5) | $\bar{x}$ = 1.2 |
| 2 | $Ti(C_{0.5},N_{0.5})$ | Fe(0.09),$O_2$(1.55), Co(0.3) | x<2 |
| 3 | $Ti(C_{0.5},N_{0.5})$ | Fe(0.15),$O_2$(0.76), Co(0.2) | 2<x<4 |
| 4 | $Ti(C_{0.5},N_{0.5})$ | FC(0.02),Fe(0.09),$O_2$(0.59),W(0.4),Co(0.03 | $\bar{x}$ = 1.28 |
| 5 | $TiB_2$ | FC(0.08, $O_2$(0.30), Co(0.2) | $\bar{x}$ = 4.5 |
| 6 | $TiB_2$ | $O_2$(0.63) Co(0.1) | $\bar{x}$ = 2.0 |
| 7 | $TiB_2$ | $O_2$(2.04) | x<2 |
| 8 | $TiB_2$ | $O_2$(0.5) | $\bar{x}$ = 1, x<4 |
| 9 | $TiB_2$ | $O_2$(1.91) | $\bar{x}$ = 1, x<4 |
| 10 | WC | FC(0.04),Fe(0.03) | $\bar{x}$ = 0.9 |
| 11 | Co | | x<2 |

Table 2. Chemical Composition and Average Particle Size of Raw Materials

| Raw material | Chemical composition (%) | Average size ($\mu$m) |
|---|---|---|
| $Ti(C_{0.5}, N_{0.5})$ | N(11.05), O(1.07) | 0.77 |
| TiC | FC(0.05) | 0.86 |
| TiN | N(21.2), TC(0.3), O(0.32) | 0.68 |
| $Cr_3C_2$ | FC(0.14), O(0.52) | 0.79 |
| $B_4C$ | Fe(0.34) | -6 sieved |

lapped face as well as the etched face of the sintered compacts using a scanning electron microscope (SEM), and through stereological point and line analyses using the photos. The measurement of transverse rupture strength was conducted using the three-point bending technique. Vickers hardness was measured using a 300 N load, and fracture toughness was calculated using Evans' and Charles' equation ($K_{IC} = 0.16\ H_{va}^{1-2}\ (c/a)^{-3/2}$). In the equation, $H_v$ denotes Vickers hardness, 2a represents the diagonal length of the impression, and 2c represents crack length in the diagonal direction of the impression.

The cutting experiment was conducted using normalized carbon steel S45C. The shapes of the cutting tools used in the experiment and cutting conditions are given in Table 3. Figure 1 shows a state of tool wear. In our experiment, VB and $VN_2$ were measured using a measuring microscope.

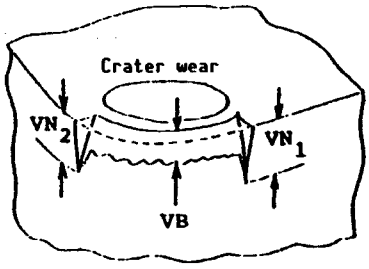


Figure 1. Typical Pattern of Tool Wear
VB = Width of flank wear
$VN_1$ = Width of side grooving wear
$VN_2$ = Width of end grooving wear

Table 3. Tool Shape and Cutting Condition

| | |
|---|---|
| Cutting type | Turning, Dry |
| Tool geometries | -5°·-5°·5°·5°·15°·15°·0.8 mm |
| Tool size | 6.35 x 6.35 x 3.18 mm |
| Cutting speed | 300 m/min |
| Feed of cutting | 0.15 m/rev |
| Depth of cutting | 0.5 mm |
| Material of workpiece | Carbon steel contained 0.15% carbon |

## 3. Experiment Results and Discussion

### 3.1 Vacuum Environment Sintering of Ti(C,N)-$TiB_2$ Powder

#### 3.1.1 Effects of $TiB_2$ Powder Grain Diameter

The density of a molded compact is believed to be affected by the grain diameter of $TiB_2$ and Ti(C,N) material powders. Among the kinds of material powders listed in Table 1, Nos. 1, 5, 6, and 8 were used for this experiment. Figure 2(A) and 2(B) show the results of measurement of transverse rupture strength and porosity vs. sintering temperature. From these results, it can be seen that the density and strength in the sintered compacts increase when the average diameter of $TiB_2$ powder decreases.

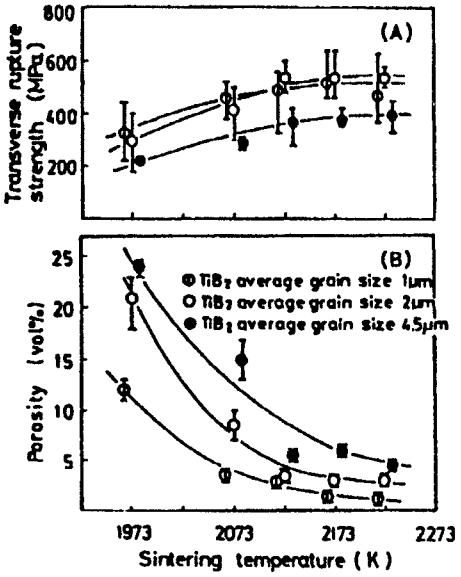


Figure 2. (A) Transverse Rupture Strength, and
(B) Porosity Vs. Sintering Temperature
The materials were sintered at each temperature for 5.4 ks in a vacuum.

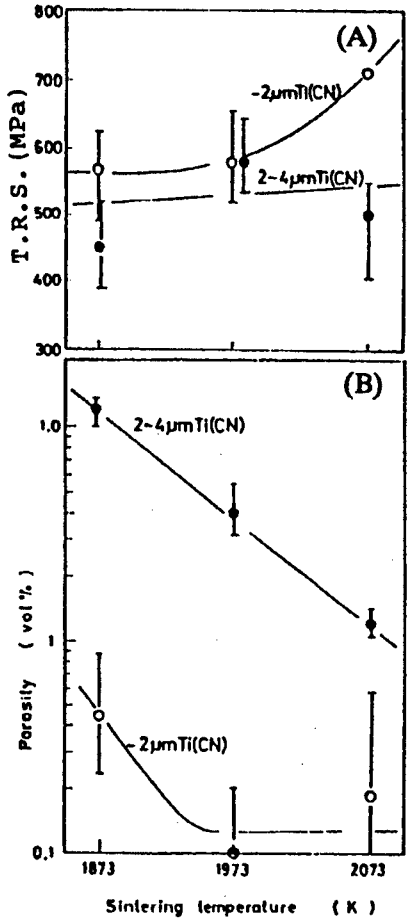


Figure 3. (A) Transverse Rupture Strength, and
(B) Porosity Vs. Sintering Temperature
The materials were sintered at each temperature for 5.4 ks in a vacuum.

### 3.1.2 Effects of Ti(C,N) Powder Grain Diameter

To see the effects of Ti(C,N) powder grain diameter on the transverse rupture strength, an experiment was conducted using materials Nos. 2, 3, and 7 in Table 1. The results are shown in Figure 3(A) and 3(B). From the figure, it can be seen that the grain diameter of Ti(C,N) powder affects the density of sintered compacts and their transverse rupture strength greatly. Figure 4 shows the crystal structure of the ceramics sintered using these powders. Gray portions represent $TiB_2$ grains and whitish portions represent Ti(C,N) grains, with black portions showing pores. From these results and observation, it can be found that the ceramics produced using small grain diameter Ti(C,N) powder has a low porosity and a high transverse rupture strength.

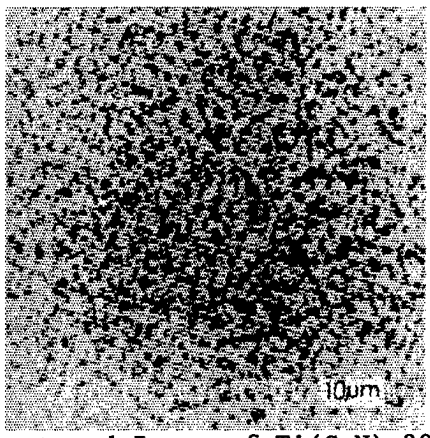


Figure 4. Back-Scattered Image of Ti(C,N)-30% $TiB_2$ Materials

### 3.1.3 Effects of Oxygen Contained Within $TiB_2$ Powder

The surface of $TiB_2$ powder can be oxidized fairly easily during material powder mixing. Considering this, we have studied the effects of oxygen on the strength of sintered ceramics and the porosity using material powders numbered 1, 8, and 9 listed in Table 1. Table 4 shows that the oxygen contained within $TiB_2$ powder affects the porosity and the transverse rupture strength in the sintered compacts greatly. At the sintering temperature, a chemical reaction, indicated as $2TiB_2 + 5O_2 \rightarrow TiO_2 + 2B_2O_3$, is known to occur. It is believed that the $B_2O_3$ that evaporates at the high temperature experienced in the sintering is responsible for the generation of pores.

Table 4. Porosity and Transverse Rupture Strength of Ti(C,N)-30% $TiB_2$ Sintered Materials Using Different Oxygen Content

| Oxygen content of raw $TiB_2$ powder (Wt%) | Temperature rupture strength (MPa) | Porosity (vol%) |
|---|---|---|
| 0.5 | 560 | 1.8 |
| 1.9 | 450 | 8.8 |

### 3.2 Vacuum Sintering of Ti(C,N)-$Cr_3C_2$ Powder

As described above, $TiB_2$ is effective as a sinter promotion agent in sintering Ti(C,N) powder. However, in producing a high-density Ti(C,N)-$TiB_2$-system ceramics by sintering the powder in a vacuum environment, the sintering temperature reaches as high as 2,123 K. This makes it necessary to develop a new sinter promotion agent that allows sintering at a lower temperature, when the ceramics is used in industrial applications. On the other hand, study is being made to use TiC-$Cr_3C_2$-system powder to produce ceramics. However, the role that $Cr_3C_2$ pays as a sinter promoting agent within TiN and Ti(C,N) powders must be studied further before it can be used with TiC powder.

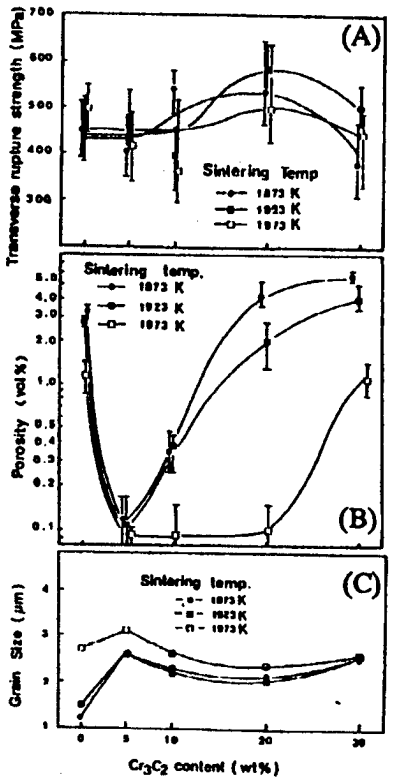


Figure 5. $Cr_3C_2$ Content Vs. (A) T.R.S., (B) Porosity, and (C) Ti(C,N) Grain Size of Ti(C,N)–a%$Cr_3C_2$ Materials Sintered at 1,873 K, 1,923 K, and 1,973 K in a Vacuum

With this in mind, we tried first to clarify further the sinter characteristics of Ti(C,N)–$Cr_3C_2$–system ceramics. Then we tried to improve the density in TiC–$Cr_3C_2$–, TiN–$Cr_3C_2$–, and TiC–TiN–$Cr_3C_2$–system ceramics by studying the sinter characteristics of these ceramics. In addition, we studied the effects of adding $B_4C$ as a sinter promotion agent.

### 3.2.1 Effects of Addition of $Cr_3C_2$ on Porosity and Transverse Rupture Strength

Figures 5(A), 5(B), and 5(C) indicate the relationship between $Cr_3C_2$ volume as a sinter promotion agent and the transverse rupture strength, $Cr_3C_2$ volume and porosity, and $Cr_3C_2$ volume and Ti(C,N) powder grain size, respectively. From the figures it can be seen that a high-density sintered compact can be obtained by adding a 5 wt%$Cr_3C_2$ and sintering at temperatures ranging from 1,873~1,973 K. Figure 6(A) shows the microstructure in one of the sintered compacts produced under the said conditions. It can be seen that a high density has been achieved and no chromium carbide phase can be observed. An X-ray analysis found the peak only at the location of cubic Ti(C,N), indicating a possibility of the Ti(C,N) phase transforming into a (Ti,Cr)(C,N) phase. Figure 7 shows the relationship between the amount of a residual chromium carbide phase within a sintered compact and porosity. From the figure it can be found that porosity increases when the residual chromium carbide phase increases, while porosity decreases when sintering temperature increases.

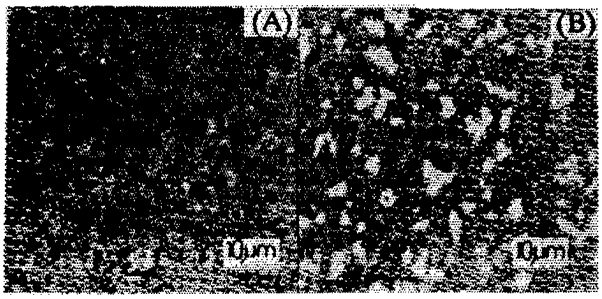


Figure 6. Microstructures of (A) Ti(C,N)–5%$Cr_3C_2$ Materials Sintered at 1,923 K and (B) Ti(C,N)–20%$Cr_3C_2$ Materials Sintered at 1,923 K in a Vacuum

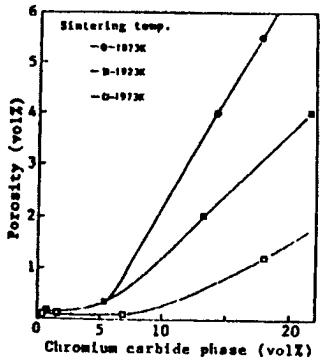


Figure 7. Chromium Carbide Phase Content in Sintered Materials Vs. Porosity

From these results, it can be said that the increase of porosity when $Cr_3C_2$ contents are boosted from 10 wt% to 30 wt% (Figure 5(B)) has something to do with an increase of residual chromium carbide within a sintered compact. It can also be seen that when $Cr_3C_2$ contents stand at 5 wt%, the residual chromium carbide phase remains lower than 1 vol% at a sintering temperature between 1,873~1,973 K, with porosity remaining below 0.3 vol%.

In Figure 5(A), a high-density sintered compact produced by adding 5 wt%$Cr_3C_2$ had a transverse rupture strength of about 450 MPa. The sintered compact that had a higher porosity with the addition of a 20 wt%$Cr_3C_2$ displayed a higher transverse rupture strength. The possible reason for the improved rupture strength will be discussed below.

We found that the diameter of Ti(C,N) grains ranged from 2.6~3.1 $\mu$m when the $Cr_3C_2$ contents stood at 5 wt%, and the diameter decreased when the contents were increased to 10 wt% to hit the bottom at 20 wt% (Figure 5(C)). From this observation, we believe the reason for the maximal level of transverse rupture strength despite an increase of porosity as a result of increase of $Cr_3C_2$ contents to 20 wt% has something to do with the grain diameter of Ti(C,N) powder. To find the reason for the increased rupture strength, we also studied the sintered compacts from a structural and compositional viewpoint. Figure 6(B) shows the microstructure of a sintered compact that reveals white chromium carbide grains scattered across the microstructure image. An X-ray analysis found that the chromium carbide is made up of $Cr_3C_2$, $Cr_7C_3$, and $Cr_{23}C_6$. From electron probe microanalyzer (EPMA) results shown in Figure 8, we believe that the material powder Ti(C,N) transforms into (Ti,Cr)(C,N) after sintering. From these observations, we believe the formation of a (Ti,Cr)(C,N) phase and the dispersion of chromium carbide grains among the material powder grains to be another reason for the improved transverse rupture strength with the addition of a 20 wt% $Cr_3C_2$. Hardness in Ti(C,N)–$Cr_3C_2$–system sintered compacts ranged from 1,800~2,000 Hv with the $K_{IC}$ value ranging from 2~3 $Mpam^{1/2}$.

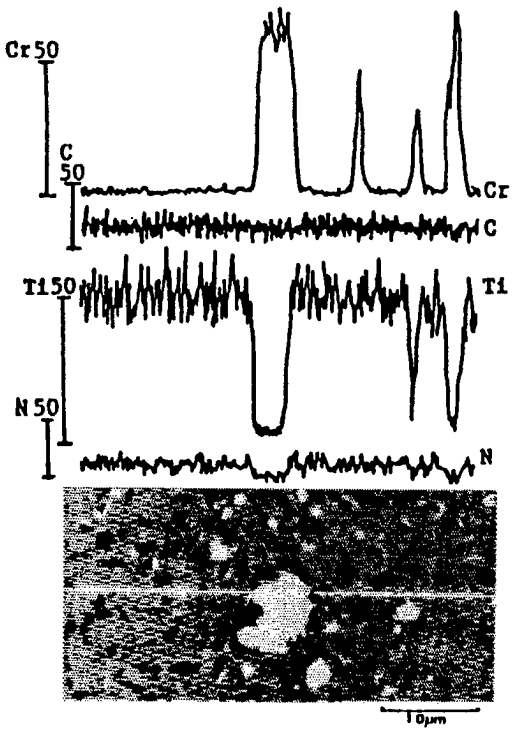


Figure 8. EPMA Line Analysis Result for Ti(CN)–10%$Cr_3C_2$ Material Sintered at 1,923 K in a Vacuum

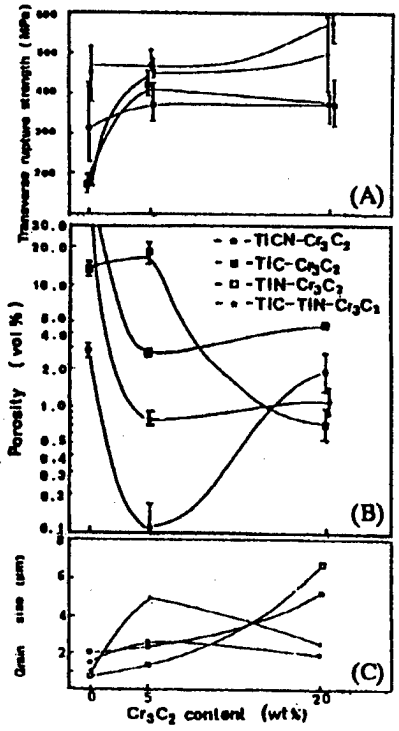


Figure 9. $Cr_3C_2$ Content Vs. (A) T.R.S. and (B) Porosity, and (C) Grain Size of Ti(C,N)–$Cr_3C_2$, TiC–$Cr_3C_2$, TiN–$Cr_3C_2$, and TiC–TiN–$Cr_3C_2$ Materials Sintered at 1,923 K in a Vacuum

### 3.2.2 Comparison Between Ti(C,N), TiC, TiN, and TiC-TiN

Figures 9(A), 9(B), and 9(C) show the effects of $Cr_3C_2$ contents on the porosity, transverse rupture strength, and grain size in sintered compacts. Figures 10(A), 10(B), 10(C), and 10(D) show the microstructures of the sintered compacts. From these data, it can be seen that at 5 wt%$Cr_3C_2$ transverse rupture strength peaks when the same material powder is used. Figure 9(C) would explain the reason for the highest rupture strength. A comparison of grain size between Ti(C,N), TiC, and TiN powders at a $Cr_3C_2$ content of 20 wt% revealed that the average diameter of Ti(C,N) powder in Ti(C,N)–$Cr_3C_2$–system material was the smallest. In TiC–$Cr_3C_2$– and TiN–$Cr_3C_2$–system sintered compacts, no residual chromium carbide phase was detected. It is believed that this resulted in the larger grain diameters in the compacts. When a comparison was made between TiC–TiN–$Cr_3C_2$–system compacts and Ti(C,N)–$Cr_3C_2$–system compacts, in both of them a chromium carbide phase was detected and the $Cr_3C_2$'s efficiency in restraining grain growth was higher in Ti(C,N)–$Cr_3C_2$ powder.

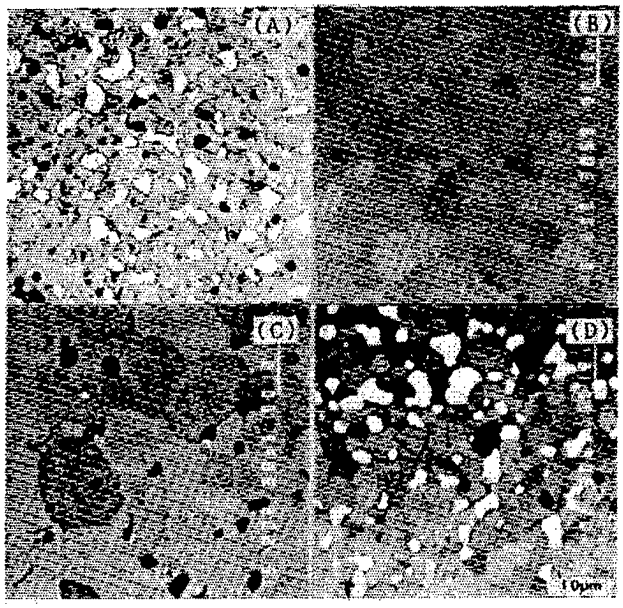


Figure 10. Back-Scattered Images of (A) Ti(C,N)-20%$Cr_3C_2$, (B) TiC-20%$Cr_3C_2$, (C) TiN-$Cr_3C_2$, and (D) TiC-TiN-20% $Cr_3C_2$ Ceramics Sintered at 1,873 K for 5.4 ks in a Vacuum

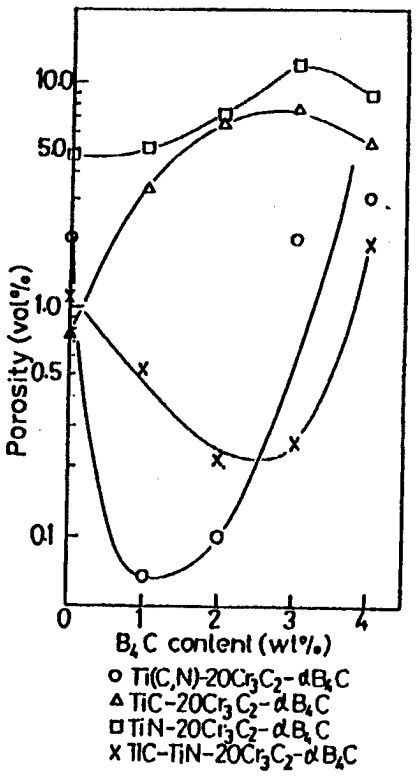


Figure 11. Relationship Between $B_4C$ Content and Porosity of the Sintered Materials The materials were sintered at 1,923 K for 90 minutes in a vacuum.

### 3.2.3 Effects of $B_4C$ to the Properties of Sintered Compacts

As described above, introduction of a 20 wt%$Cr_3C_2$ into Ti(C,N) and TiC-TiN powders produces a residual chromium carbide phase and pores within the sintered compacts produced using these powders. Figure 11 shows the effects of adding $B_4C$ on the porosity of sintered compacts. In the compacts produced using Ti(C,N)-20 wt%$Cr_3C_2$- and TiC-TiN-20 wt%$Cr_3C_2$-system powders a residual chromium carbide phase was found, and in the compacts porosity decreased when $B_4C$ was added. Particularly, the decrease was marked in Ti(C,N)-20 wt%$Cr_3C_2$-system sintered compacts. Figure 12 shows the microstructure of one of the compacts. An X-ray analysis indicates the possibility that part of the $B_4C$ powder grains reacted with the $Cr_3C_2$ to transform into CrB2.

### 3.3 Evaluation of Cutting Capability

Figure 13 gives the relationship between VB values and cutting times in a number of kinds of ceramics when a cutting capability evaluation test was conducted under a cutting speed of 300 m/min.

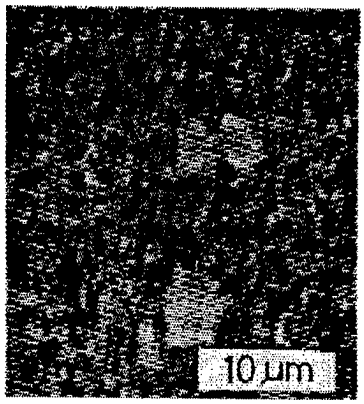


Figure 12. Backscattered Image of Ti(C,N)–20%$Cr_3C_2$–2%$B_4C$ Ceramics. The ceramics were sintered at the temperature of 1,873 K for 5.4 ks in a vacuum.

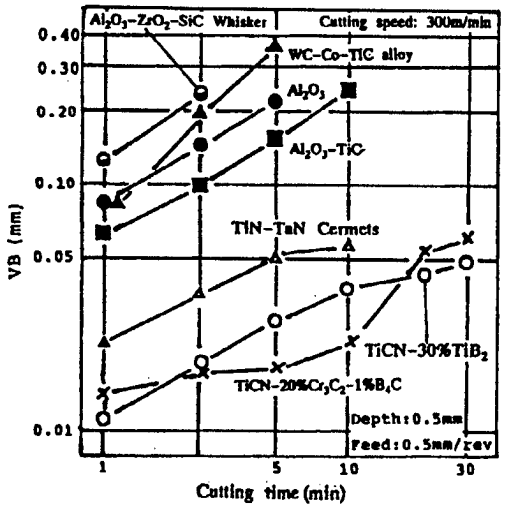


Figure 13. VB Vs. Cutting Time

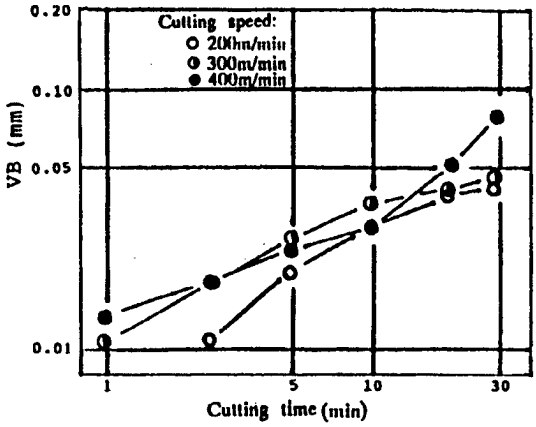


Figure 14. VB Vs. Cutting Time

Figure 14 gives the results of the measurement of VB when cutting was conducted using Ti(C,N)–30 wt%$TiB_2$ tools at cutting speeds of 200, 300, and 400 m/min. At 300 m/min, both Ti(C,N)–20 wt%$Cr_3C_2$–1 wt%$B_4C$ tools and Ti(C,N)–30 wt%$TiB_2$ tools displayed higher antiwear capabilities than conventional tools. At cutting speeds between 200~400 m/min, a small degree of boundary wear $VN_2$ was observed in Ti(C,N)–30 wt%$TiB_2$ tools. However, they also exhibited superior antiwear capability in the cutting speed range.

**Epilogue**

Following is the summary of the result of our research in which we produced Ti(C,N) ceramics using $TiB_2$ and $Cr_3C_2$ as sinter promotion agents by sintering the mixture of the material powder and the sinter promotion additives in a vacuum, and studied the characteristics of the sintered compacts and the capabilities of the cutting tools produced using the ceramics.

(1) $TiB_2$ powder was found to serve as an effective sinter promotion agent when used with Ti(C,N) powder. The density and transverse rupture strength in Ti(C,N)-30 wt%$TiB_2$-system ceramics were affected greatly by the grain diameters of $TiB_2$ and Ti(C,N) powders and oxygen contents within the sinter promotion agent.

(2) Ti(C,N)-$Cr_3C_2$-system powder allows obtaining a sintered compact at a relatively low sinter temperature, and $Cr_3C_2$ can be used as an effective sinter promotion agent. When $B_4C$ powder was added to Ti(C,N)-20 wt%$Cr_3C_2$-system powder at a rate ranging from 1~3 wt%, porosity in the sintered compacts decreased greatly.

(3) In cutting S45C carbon steel samples, Ti(C,N)-30 wt%$TiB_2$-system tools and Ti(C,N)-20 wt%$Cr_3C_2$-1 wt%$B_4C$-system tools displayed higher antiwear capabilities than conventional tools.

- END -